Use of individual wheel steering to improve vehicle stability and disturbance rejection

by

Richard C.K. Nkhoma

Submitted in partial fulfilment of the requirements for the degree

MSc (Applied Science) Mechanical

in the Faculty of

Engineering, Built Environment and Information Technology

University of Pretoria, Pretoria

October 2009

Use of individual wheel steering to improve vehicle stability

and disturbance rejection

By

Richard C.K. Nkhoma

Supervisor : Prof. N.J. Theron

Department : Mechanical and Aeronautical Engineering

Degree : MSc (Applied Science) Mechanical

ABSTRACT

The main aim of this research project is to extend theories of four-wheel-steering as developed by J. Ackermann to include an individually steered four-wheel steering system for passenger vehicles. Ackermann's theories, including theories available in this subject area, dwell much on vehicle system dynamics developed from what is called single track model and some call it a bicycle model. In the bicycle model, the front two wheels are bundled together. Similarly, the rear wheels are bundled together. The problem with this is that it assumes two front wheels or two rear wheels to be under the same road, vehicle and operating conditions. The reality on the ground and experiments that are conducted are to the contrary. Therefore this study discusses vehicle disturbance rejection through robust decoupling of yaw and lateral motions of the passenger vehicle.

A mathematical model was developed and simulated using Matlab R2008b. The model was developed in such a way that conditions can be easily changed and simulated. The

model responded well to variations in road and vehicle conditions. Focus was in the ability of the vehicle to reject external disturbances. To generate yaw moment during braking, the brake on the left front wheel was disconnected. This was done because lateral wind generators, as used by Ackermann, were not available. The results from both simulations and experiments show disturbance rejection in the steady state.

Keywords – Disturbance rejection, yaw rate, lateral acceleration, four wheel steering (4WS), individual wheel steering (IWS), robust control, robust decoupling.

ACKNOWLEDGEMENT

I would like to thank, Prof N. J. Theron, who not only served as my supervisor but also encouraged and challenged me throughout my academic program and whose tireless efforts and his ever present helping hand made this work a success. I would also like to thank Prof. S. Els for his invaluable comments and inputs, and not forgetting my office mate and now Dr. Michael Thoreson who tried all he could to supply solutions to all my academic questions.

To my wife Catherine and child Peace for their encouragement and love despite the long distance that separated us. You were a source of inspiration to me in times when the chips were down.

To all friends too many to mention, I just want to say that thank you for all the moral support that you rendered to me during my study, particularly I would like to thank Jimmy Mokhafera for his support during the whole period of my research. May the Good LORD richly bless you all.

Above all, I would like to thank God through Jesus Christ for HIS mercies and grace towards me throughout my stay in South Africa.

TABLE OF CONTENTS

LIST OF FIGURES

LIST OF TABLES

NOMENCLATURE

α_i individual wheel slip angle

α_1 front left slip angle

α_2 front right slip angle

α_3 rear left slip angle

α_4 rear right slip angle

a_x longitudinal acceleration

a_y lateral acceleration

a_{yDP} lateral acceleration at decoupling point

a distance the front axle is ahead of the centre of gravity (i.e., negative if the centre of gravity lies ahead of the front axle)

A state dynamic matrix

A_f frontal area of the vehicle

β chassis sideslip

β_i chassis sideslip angle at individual wheel position

β_1 chassis sideslip angle at front left wheel

β_2 chassis sideslip angle at front right wheel

β_3 chassis sideslip angle at rear left wheel

β_4 chassis sideslip angle at rear right wheel

B state input matrix

$C_{\alpha i}$	individual wheel cornering stiffness
$C_{\alpha 1}$	front left wheel cornering stiffness
$C_{\alpha 2}$	front right wheel cornering stiffness
$C_{\alpha 3}$	rear left wheel cornering stiffness
$C_{\alpha 4}$	rear left wheel cornering stiffness
C	state output matrix
C_{dx}	longitudinal drag coefficient
C_{dy}	lateral drag coefficient
C_{Mz}	yaw moment coefficient
C_{Fy}	lateral force coefficient.
δ_i	individual wheel steering angle
δ_1	front left steering input (driver and control inputs)
δ_2	front right steering input (driver and control inputs)
δ_3	rear left steering input
δ_4	rear right steering input
δ_c	control steering input
δ_f	steering wheel angle
δ_s	part of the front wheel steering angle that is the same for the left and right wheels and is directly controlled by the driver
D	state input output coupling matrix

F_{dx} — longitudinal disturbance force , assumed to be acting through the centre of pressure.

F_{yi} — individual wheel force in the vehicle body axis system y direction

F_{xi} — individual wheel force in the vehicle body axis system x direction

F_{dy} — lateral disturbance force , assumed to be acting through the centre of pressure

F_x — summation of all longitudinal forces

F_y — summation of all lateral forces

F_{xti} — longitudinal wheel forces on the individual wheels axis system

F_{yti} — lateral wheel forces on the individual wheels axis system

γ_i — corrective individual slip angle for front wheels only

h_{cg} — height to centre of gravity

K_i — generic gain parameter, where the index i is used to identify the gain in the text.

I_z — moment of inertia about z axis

l — wheelbase

l_f — distance the front axle is ahead of the centre of pressure (i.e., negative if the centre of pressure lies ahead of the front axle)

l_{gp}	distance the centre of pressure is ahead of the centre of gravity (i.e., negative if the centre of pressure lies behind the centre of gravity)
l_{gm}	distance the centre of the vehicle is ahead of the centre of gravity
l_{mp}	distance the centre of pressure is ahead of the centre of the vehicle
l_r	distance the centre of gravity is ahead of the rear axle
m	total mass
M_{z_i}	self aligning torques
M_{z_e}	generic torques that are applied to the wheels
μ	friction coefficient
r	yaw rate and is the same as $\dot{\psi}$
r_{ref}	reference yaw rate
r_{def}	the difference between reference yaw rate and the actual yaw rate
t	half track width of the vehicle
t	time
θ	the angle of road inclination in the direction of travel.
θ	sprocket angle.
$\boldsymbol{u}$	state input vector
v	vehicle velocity
v_x	longitudinal velocity

v_y	lateral velocity
v_{wr}	resultant wind velocity
v_{wy}	crosswind velocity
$x_0 - y_0$	horizontal plane of an inertial axis system (as in figure 3-1)
$x - y$	horizontal plane of a vehicle body fixed axis system, x forward (longitudinal), y lateral.
y	state output vector
ψ	yaw angle
z	vertical plane of the vehicle axis system, positive downwards

1   INTRODUCTION

1.1   *Background*

The concept of four wheel steering (4WS) in motor vehicles is manifested when the driver is able to steer both front and rear wheels. There are several methods that have been investigated in order to achieve 4WS, as noted in the literature review. There are various reasons that necessitated the research into 4WS, like sudden disturbances rejection (e.g. side wind forces, sudden wheel burst, rough roads, μ-split), improving steerability and stability of vehicles and to increase ride comfort for the driver and passengers.

Research of four-wheel car steering system has gained much attention from the early 1980's. Since then, there has been a tremendously growing interest in the research and development of 4WS. Early systems used simple open loop architecture to achieve active control. To date several attempts have been made to improve handling characteristics and performance of vehicles in order to increase manoeuvrability, stability, safety, and ride comfort.

The use of single-track model to analyse the fundamentals of steering dates back as early as 1940 as pointed out by Ackermann et al. (2002). This method assumes that steering angles are the same for the two front wheels as well as for the two rear wheels. It is used much in literature for the derivation of equations.

This research focuses on an extension of Ackermann's theory, mainly as given by Ackermann et al. (2002), to develop a system that would enable all wheels to be steered individually. In addition to allowing each wheel to rotate through a steering angle, each

wheel is also equipped with a linear actuator to effect steering. The steering signal from the driver is the conventional angular input using the steering wheel. The total steering angle for a front wheel will thus be made up of the input from the driver and the angle generated by the actuator. As for the rear wheels, the input angles will come from the actuators only. The actuators are controlled by a control system, independently of the driver. The purpose of this control system is to react to and reject suddenly applied disturbances in the short delay period caused by the driver's slow reaction time, but then to return control to the driver.

1.2   *Statement of the Problem*

This research analysed steering performance characteristics of a certain vehicle for all speed ranges, i.e. at low speeds as well as at high speeds. Therefore this study concentrated on theoretical and experimental analysis of the steering performance characteristics of the vehicle under the above-mentioned conditions. This was done in order to improve the current vehicle handling characteristics, manoeuvrability, stability, safety, and to increase ride comfort for the driver as well as the passengers. Measurements on the developed system indicated steady state rejection of disturbances. Work of the previous researchers was investigated in order to assess the current level of performance of 4WS as outlined in the subsequent chapters.

1.3   *Approach*

Theoretical modelling and analysis of individual wheel steering (IWS) was done when all information was gathered both from available literature as well as from the existing 4WS experimental vehicle in the SASOL Laboratory.

After developing the necessary theory, computer simulations were done and all information gathered was applied to the experimental vehicle to observe the actual performance. Therefore this research involved three sections:

- Theoretical modelling and analysis of an IWS vehicle.

- Computer simulations of an IWS vehicle.

- Physical implementation and modifications on the existing four-wheel car steering system, followed by road tests to evaluate the effects of modifications.

Figure 1-1 shows a standard SAE vehicle axis system and terminology as defined by SAE J670e (1976). These are used throughout this work in the theoretical dynamic modelling. The directions are as defined in the nomenclature.
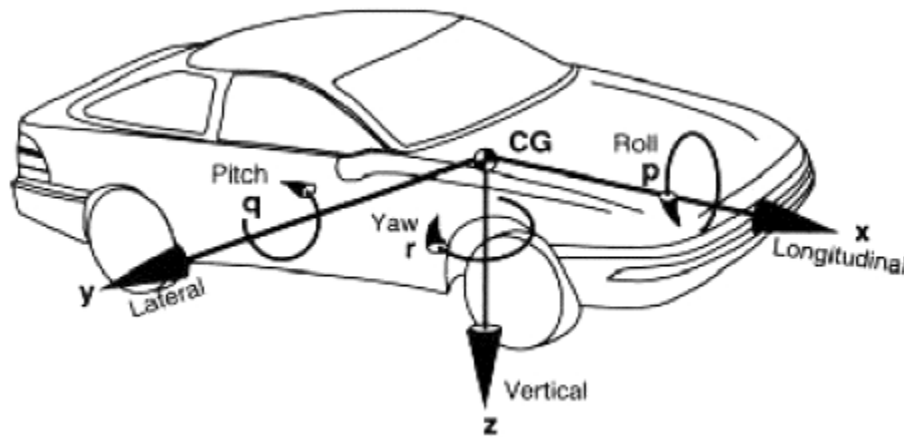
Figure 1-1:   SAE Vehicle axis system notations (SAE J670e (1976))

2   LITERATURE REVIEW

2.1   *Experimental Vehicle Status*

The experimental 4WS vehicle that is available in the SASOL laboratory of the University of Pretoria was designed and built by Burger in 1995. Klein (1996) used this vehicle to study the optimisation of the phase shift in all wheel steering to minimize the percentage overshoot on yaw velocity. He used active control system theory to achieve active control of the vehicle's steering system.

2.2   *Current Research Situation*

Different researchers have suggested various ways of achieving good characteristics and handling performance of 4WS vehicles. Below are some of the suggested and implemented methods, as found in the literature, from control point of view since the focus of this research will mainly be on control issues.

2.2.1   *Decoupling controller*

Ackermann et al. (2002) (in particular chapter 6), make good observations and analyses of the 4WS system. They firstly identify and then discuss decoupling two steering tasks, for the purpose of improved steering control and disturbance rejection. One of the tasks is to be performed by the driver, which is path tracking. The other steering task is done by the automatic control system to counter the effect of disturbance. This automatic control system is thought to do the disturbance rejection faster and more precise than the driver. They achieved their desired robust decoupling effect by cancellation of the yaw rate through a feedback control law. This makes the yaw rate non-observable from the lateral acceleration at the decoupling point. They showed through experiments that their

robust control system reduces the yaw rate to zero and then the driver, as his path tracking task, returns the vehicle to the original heading.

The robust decoupling control concept is practically useful, only if the resulting subsystems are stable, or can be stabilised separately without destroying the decoupling effect. Some of the work about decoupling is also given in the papers presented by Ackermann et al. (1992, 1995, 1996, 1997 and 2004).

Ackermann et al. (1999) say that there were some items that were not satisfactory in the actual driving experiments through the use of robustly decoupling control. The first one was that damping of the separated yaw dynamics was not sufficient at high speeds. The second drawback was that integral feedback had been implemented only to achieve robust unilateral decoupling despite providing steady state accuracy. The last drawback outlined was that limit cycles happened due to actuator rate limitations.

2.2.2 *Drive by wire*

Klein (1996) advocated the use of steer (drive) by wire. Lynch (2000) says that with drive by wire, no mechanical restrictions exist in choosing the front and rear steering angles and that the driver has no direct control over any of the wheels. In this kind of steering, the steering wheel has no direct physical connections to the wheels. All steering angles are supposed to be determined by an onboard computer. One of the advantages of drive by wire is that there is tremendous flexibility in designing the handling characteristics of the vehicle. Klein (1996) applied in his research a strategy of yaw rate feedback to control rear steering

angles through the use of a controller, and driver input to control front steering angles. Despite all this, drive by wire has its disadvantages and the obvious one is the potential for disaster from controller failure as outlined by Lynch (2000).

2.2.3   Driver assisted control

Lynch (2000) proposes a concept of driver-assisted control (DAC) where the driver has full command of the front wheel steering angle mechanically through the steering wheel. He uses a flexible controller to improve the vehicle performance by steering the rear wheels while allowing the driver to take full charge in the event of controller failure. He incorporates the ideas behind drive by wire and driver assisted control to achieve his goals.

The drawback is that his simulations focussed on low speeds in the range of 1 to 4 m/s. His system was more oscillatory at higher speeds and this seems to suggest that the system was moving towards instability at higher speeds.

2.2.4   Adaptive Steering Controller

Wu et al. (2001) used an adaptive controller for achieving accurate and prompt control with noisy steering command signals and drifting valve characteristics on an automated agricultural tractor with electro-hydraulic steering system. The adaptive controller consisted of a feedforward base controller, a proportional-integral-derivative (PID) base controller; a Kalman filter based adaptive (PID) gain tuner, a wheel angle estimator and an adaptive nonlinearity compensator. In this design, the feedforward controller determines the primary control signal on

the demand steering angle, and the PID controller provides a compensation signal to offset the steering error based on the feedback signal.

The draw back in the adaptive control system is that there is a need to have a process to identify real time vehicle response variables as pointed out by Abe (1999, 2002). The problem then comes when the steering input from the driver is very small, in which case the accuracy of the identification will deteriorate. On top of that, the theoretical treatment of stability conditions for designing an adaptive control system is complicated. To address these problems Wu focussed on direct yaw moment control (DYC), where vehicle motion is controlled by a yaw moment actively generated by the intentional excitation of wheel longitudinal forces.

2.2.5 H_2 / H_∞ *synthesis*

Kitajima et al. (2000) used H_∞ control as an integral part of their design, which optimises the control inputs and goals with predictable disturbances. In their design, the front steering angle is considered as a detectable disturbance, whose effect was to be rejected by the control signal. Their first integration design is a feedforward integration type. In this design, one vehicle control input is designated for each vehicle output and the other control inputs were treated as disturbances. In order to study the effectiveness of these two integration designs, a simulator, which realises vehicle longitudinal, lateral, roll, yaw and each wheel rotational motion, was developed. In order to improve vehicle handling and stability at high speeds, a multiobjective H_∞ optimal control was investigated by

Lv et al. (2004) based on yaw rate tracking. In particular, the four wheel steering vehicle is controlled to simultaneously stabilise the responses of yaw rate, side slip angle and lateral acceleration to the front wheel steering angle with the rear wheels steered by wire.

You and Joeng (1998) designed an autopilot of a four-wheel steering vehicle against external disturbances. To enhance the dynamic performance of this automobile system, a mixed H_2 / H_∞ synthesis with pole constraint was designed on the basis of a full state feedback applying linear matrix inequality (LMI) theory. For lateral/directional and roll motions, the steering angles were actively controlled by steering wheel angles through the actuator dynamics.

Although the H_2 approach is well suited to many real systems, it is known that its stability and robustness cannot be guaranteed in the presence of various uncertainties as pointed out by You and Joeng. As is the case with many vehicle systems, a passenger car is expected to operate in a highly variable environment and can be affected by fluctuations under manoeuvring conditions. This raises questions about robustness of the control system by which the vehicle controller must cope with these uncertainties successfully. They pointed out that H_∞ synthesis guarantees a robust stability and disturbance rejection performance in the presence of uncertainties. The drawback is that the H_∞ optimal controller typically leads to an intolerable large control effort. To trade off, they combined the two H_2 and H_∞ effects to come up with H_2 / H_∞ synthesis with pole constraint via LMIs.

2.3   *Closing*

Some of the methods in the literature are tailored towards a particular variable. Various researchers try to achieve better vehicle handling characteristics by designing controllers for a specific situation like disturbance input from side wind forces or μ split, etc. So far the solutions given in the literature are based on simplified and linearized models of the vehicle systems. The drawback to this is that it is not possible to predict road conditions.

In this study, existing solutions have been analysed and incorporated to achieve better vehicle handling performance characteristics and stability and to reject external disturbances. Some of the variables neglected in most of the literature were considered. This study wanted to specifically perform an investigation similar to what Ackerman, et al. (2002) have done, but with a difference that instead of using a bicycle model, the model used in this work has the two wheels on the same axle modelled separately, with different conditions and the possibility for different steer angles and control signals. The theory that was developed by Ackerman, et al. (2002), allows the control system to reject disturbances caused by the two wheels on the same axle not experiencing the same conditions, as illustrated by some of the experiments described in this book, like μ-split braking. This theory works well for that case even though he does not model the left and right wheels separately, and that illustrates the robustness of this theory. Furthermore, this work will investigate whether modelling and controlling the left and right wheels separately would not further improve the theory by Ackerman, et al. (2002), and to investigate the benefits (or not) of having the possibility to have different control steering angles at each of the four wheels. In the analysis, aerodynamic drag will be considered and that the vehicle will be assumed to be travelling at constant speed.

3   MATHEMATICAL MODELLING

3.1   *Introduction*

To understand the behaviour of the vehicle at the point of turning, a model was developed and using this model, equations of motion were derived. There are various methods of achieving four-wheel vehicle steering as outlined by Lakkad (2004) and there are also different ways of building models as well as ways of working on these models. In this work, nonparallel steering was used for derivation of the equations of motion. This type of steering is when the steered wheels on a single axle are not parallel during steering. It has been chosen in order to achieve individual wheel steering where each wheel can be steered towards the desired direction.

Figure 3-1 shows a scenario whereby the rear wheels turn in the same direction as the front wheels. The direction of a positive steer angle δ is indicated for each of the wheels in figure 3-1. The sketch shows the vehicle momentarily rotated at an angle ψ with respect to the $x_0 - y_0$ axis system.

The vehicle will exhibit translational motion as well as rotational motion during a turning manoeuvre. To describe the motion of the vehicle instantaneously, it is convenient to use extra axes, fixed to and moving with the vehicle. With respect to the latter axes, the mass moments of inertia of the vehicle are constant, where as with respect to the axes fixed in space, the mass moment of inertia varies as the vehicle changes orientation, Wong (1993). The $x - y - z$ axis system is the vehicle coordinate system which is fixed with its origin at the centre of gravity while $x_0 - y_0 - z$ axis system is the non-rotating coordinate

system moving with the vehicle and this is shown at time t. The vehicle has rotated from the $x_0 - y_0$ axis system to the $x - y$ axis system by an angle ψ, which is called yaw angle.

Figure 3-1 by implication shows the definition of the different wheel axis systems, which for wheel i is rotated about the z-axis through the steering angle δ_i, with respect to the vehicle coordinate system.
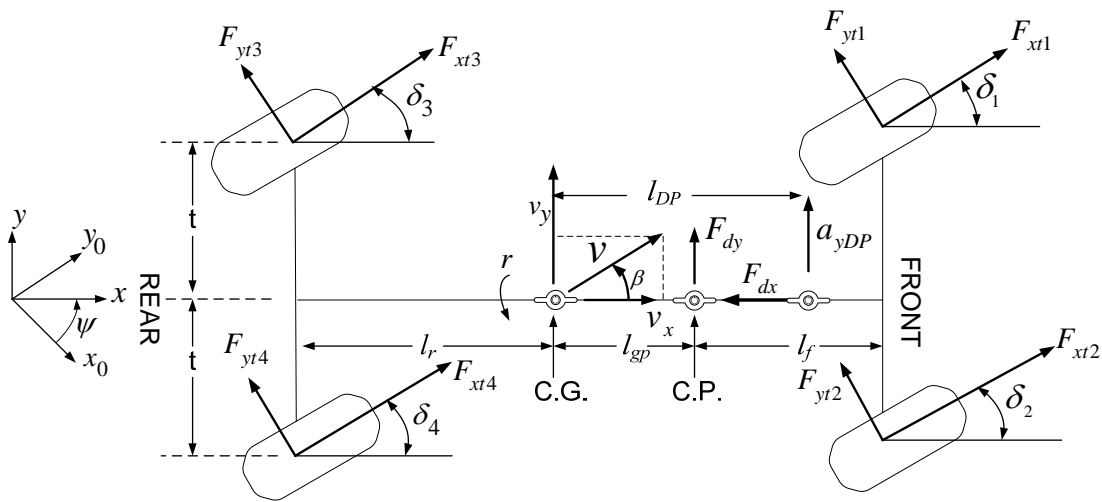
Figure 3-1:   **Wheels turning the same direction**

3.2   *Assumptions*

In order to simplify the derivation of the equations of motions, the following assumptions are made:

i.   All the analyses that will be done will assume that the vehicle is travelling or being driven at a constant speed.

ii.   The force in the x direction of the wheel axis system is sufficient to balance drag but is assumed to be significantly smaller than the lateral direction forces.

iii. The vehicle is turning at constant velocity and with this assumption acceleration in the longitudinal direction is negligible.

iv. The vehicle model to be considered is a two dimensional and rigid body vehicle.

v. The normal force of the vehicle is distributed equally onto the left and right wheels and the forces transferred by the wheels are applied in the centre of the wheel contact patch.

vi. Effects from the suspension and wheel deformation were neglected.

vii. The vehicle is travelling on a flat surface i.e. $x-y$ plane and motions to be considered occur along this plane.

viii. The vehicle is symmetrical about $x-z$ plane and the centre of pressure and the centre of gravity is in this plane.

ix. Roll, pitch and translational motion along the $z-axis$ was neglected and the remaining three degrees of freedom were considered i.e. longitudinal motion along the $x-axis$, lateral motion along the $y-axis$ and yaw motion around the $z-axis$.

x. Track width $(2t)$ at the rear is the same as at the front.

3.3 *Nonlinear vehicle model equations of motion*

In this section, equations of motion that describe individual wheel steering are derived. Referring to figure 3-1:

- Longitudinal forces for the front and rear wheels are:

$$F_{xi} = F_{xti} \cos \delta_i - F_{yti} \sin \delta_i \qquad\qquad [3.1]$$

- Lateral forces for the front and rear wheels are:

$$F_{yi} = F_{xti} \sin \delta_i + F_{yti} \cos \delta_i \qquad\qquad [3.2]$$

where $i = 1, 2, 3, 4$

The longitudinal and lateral vehicle velocities can be calculated from the actual velocity v which is at a chassis sideslip angle β to the vehicle's longitudinal axis. The corresponding acceleration components can be found by differentiating these velocities, i.e.

$$v_x = v \cos \beta \qquad\qquad \dot{v}_x = \dot{v} \cos \beta - v\dot{\beta} \sin \beta \qquad\qquad [3.3]$$

$$v_y = v \sin \beta \qquad\qquad \dot{v}_y = \dot{v} \sin \beta + v\dot{\beta} \cos \beta \qquad\qquad [3.4]$$

Let $a = \left(l_f + l_{gp} \right)$ \qquad\qquad [3.5]

Newton – Euler's laws can now be applied to figure 3-1 in order to derive equations of motion. More details about some of the derivations can be found in the books by Wong (1993), Gillespie (1992) and Genta (1997).

- *Translational motion*

  The sum of the external forces acting on the body in a given direction is equal to the product of its mass and the acceleration of the C.G. in that direction, i.e.

  - $\sum F_x = ma_x$ longitudinal motion in the x direction \qquad [3.6]

  - $\sum F_y = ma_y$ lateral motion in the y direction \qquad [3.7]

The summation of acceleration should take into account the effect of yaw rate to give a complete picture of acceleration in the x and y direction.

a. Longitudinal direction

$$\sum F_x = \sum F_{xi} - F_{d_x} = ma_x \qquad [3.8]$$

Where $F_{dx} = \frac{1}{2}\rho A_f v_{wr}^2 C_{dx}$ is typically the drag force. If the vehicle is travelling at an inclined plane, then the effect of weight in the form of $mg\sin\theta$ is added (Genta, 1997).

$$a_x = \left(\dot{v}_x - rv_y\right) \qquad [3.9]$$

$$m\left(\dot{v}_x - rv_y\right) = \sum F_{xi} - F_{d_x} \qquad [3.10]$$

Substituting for $\dot{v}_x$ and v_y from equations [3.3] and [3.4], equation [3.8] now becomes:

$$m\dot{v}\cos\beta - mv\left(\dot{\beta}+r\right)\sin\beta = \sum F_{xi} - F_{d_x} \qquad [3.11]$$

b. Lateral direction

$$\sum F_y = \sum F_{yi} + F_{d_y} = ma_y \qquad [3.12]$$

$$a_y = \left(\dot{v}_y + rv_x\right) \qquad [3.13]$$

$$m\left(\dot{v}_y + rv_x\right) = \sum F_{yi} + F_{d_y} \qquad [3.14]$$

Substituting for $\dot{v}_y$ and v_x, equation [3.12] now becomes:

$$m\dot{v}\sin\beta + mv\left(\dot{\beta}+r\right)\cos\beta = \sum F_{yi} + F_{d_y} \qquad \text{where} \quad i = 1,2,3,4 \qquad [3.15]$$

c. Rotational motion

Gillespie (1992) points out that the sum of the torques acting on a body in a given direction is equal to the product of its rotational moment of inertia about an axis through its C.G., and the rotational acceleration about that axis.

$$\sum M_z = I_z \dot{r} \qquad [3.16]$$

$$\sum M_z = a\left(F_{y1} + F_{y2}\right) - l_r\left(F_{y3} + F_{y4}\right) + t\left(F_{x2} + F_{x4} - F_{x1} - F_{x3}\right) + F_{dy}l_{gp} + M_D = I_z\dot{r}$$

[3.17]

where according to Genta (1997)

i.   As said before, F_{d_y} is the component of aerodynamic forces in the y direction. The

resulting wind velocity when driving, v_{wr}, is the combination of the apparent wind

velocity due to the vehicle's forward motion, v_x, and the cross wind velocity, v_{wy},

which is written as: $v_{wr} = \sqrt{v_x^2 + v_{wy}^2}$.

The resulting airflow has an angle of approach with respect to the vehicle, τ, which

is computed as:

$$\tau = \arctan\frac{v_{wy}}{v_x}$$

Hence:

$$F_{d_y} = \frac{1}{2}\rho v_{wr}^2 A_f C_{d_y}, \text{ (Hucho 1987, p.63).}$$

ii. M_D is made up of all the moments that are developed due to disturbance inputs i.e.

$$M_D = \sum_i M_{z_i} + \frac{1}{2}l\rho v_{wr}^2 A_f C_{M_z} + M_{z_e} \text{ (Hucho 1987, p, 63).}$$

Using equations [3.11], [3.15] and [3.17] to solve for $\dot{\beta}$, $\dot{r}$ and $\dot{v}$ gives:

$$\begin{bmatrix} -\sin\beta & \cos\beta & 0 \\ \cos\beta & \sin\beta & 0 \\ 0 & 0 & 1 \end{bmatrix}\begin{bmatrix} mv\left(\dot{\beta}+r\right) \\ m\dot{v} \\ I_z\dot{r} \end{bmatrix} = \begin{bmatrix} \sum F_{xi} - F_{dx} \\ \sum F_{yi} + F_{dy} \\ Y \end{bmatrix}$$

Where

$$Y = a\left(F_{y1} + F_{y2}\right) - l_r\left(F_{y3} + F_{y4}\right) + t\left(F_{x2} + F_{x4} - F_{x1} - F_{x3}\right) + F_{dy}l_{gp} + M_D$$

But

$$\begin{bmatrix} -\sin\beta & \cos\beta & 0 \\ \cos\beta & \sin\beta & 0 \\ 0 & 0 & 1 \end{bmatrix}^{-1} = \begin{bmatrix} -\sin\beta & \cos\beta & 0 \\ \cos\beta & \sin\beta & 0 \\ 0 & 0 & 1 \end{bmatrix}$$

therefore

$$\begin{bmatrix} mv\left(\dot{\beta}+r\right) \\ m\dot{v} \\ I_z\dot{r} \end{bmatrix} = \begin{bmatrix} -\sin\beta & \cos\beta & 0 \\ \cos\beta & \sin\beta & 0 \\ 0 & 0 & 1 \end{bmatrix}\begin{bmatrix} \sum F_{xi} - F_{dx} \\ \sum F_{yi} + F_{dy} \\ Y \end{bmatrix} \qquad [3.18]$$

3.4 Sideslip angles

Wheel slip angle α is defined as the angle that is so formed between the x – axis of the wheel axis system and the actual direction of the wheel velocity, while the sideslip angle β is the angle between the vehicle's actual velocity vector v and the vehicle axis x. Figure 3-2 shows individual wheel sideslip angles as well as the front and rear chassis sideslip angles.
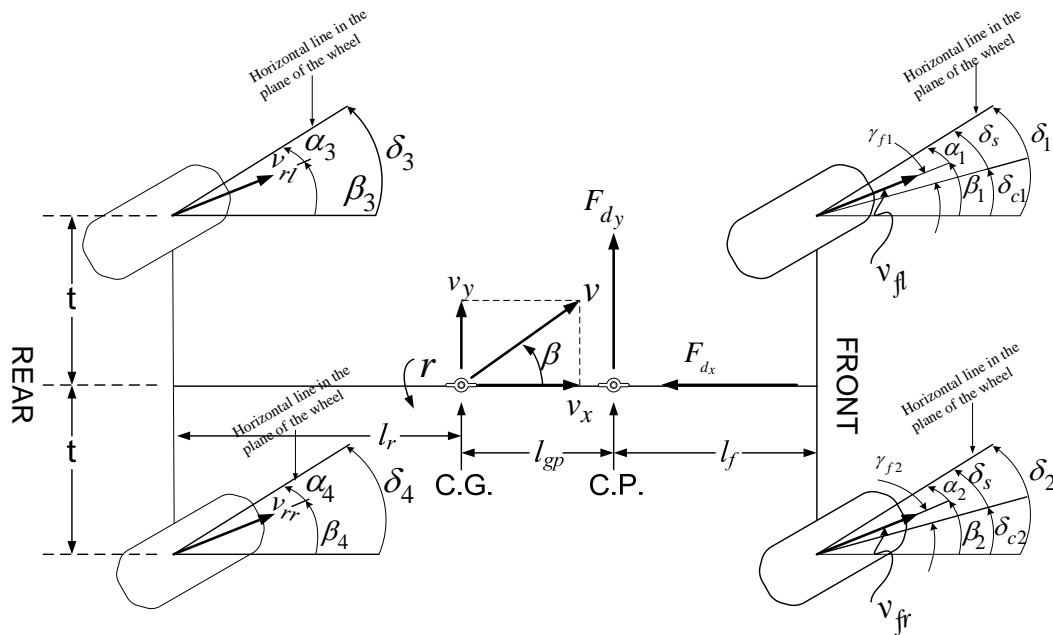

Figure 3-2: **Sketch showing wheel sideslip angles**

From figure 3-2, it can be noted that:

$$\alpha_i = \delta_i - \beta_i \text{ where } i = 1, 2, 3, 4 \qquad [3.19]$$

and that

$$\alpha_i = \delta_s - \gamma_i \text{ where } i = 1, 2 \text{ for front wheels.}$$

For the calculation of sideslip angles, the equations listed below were used as reported by Ghelardoni (2004) as well as Zhengqi et al. (2003) and are modified according to this work. Referring to figure 3-2:

$$\tan(\delta_1 - \alpha_1) = \frac{v_y + ar}{v_x - tr} = \tan \beta_1 \qquad [3.20]$$

$$\tan(\delta_2 - \alpha_2) = \frac{v_y + ar}{v_x + tr} = \tan \beta_2 \qquad [3.21]$$

$$\tan(\delta_3 - \alpha_3) = \frac{v_y - l_r r}{v_x - tr} = \tan \beta_3 \qquad [3.22]$$

$$\tan(\delta_4 - \alpha_4) = \frac{v_y - l_r r}{v_x + tr} = \tan \beta_4 \qquad [3.23]$$

From where the individual wheels sideslip angles can be found to be:

$$\alpha_1 = \delta_1 - \tan^{-1}\left(\frac{v \sin \beta + ar}{v \cos \beta - tr}\right) \qquad [3.24]$$

$$\alpha_2 = \delta_2 - \tan^{-1}\left(\frac{v \sin \beta + ar}{v \cos \beta + tr}\right) \qquad [3.25]$$

$$\alpha_3 = \delta_3 - \tan^{-1}\left(\frac{v \sin \beta - l_r r}{v \cos \beta - tr}\right) \qquad [3.26]$$

$$\alpha_4 = \delta_4 - \tan^{-1}\left(\frac{v \sin \beta - l_r r}{v \cos \beta + tr}\right) \qquad [3.27]$$

3.5   *Lateral forces*

Lateral forces that are developed at the contact patch between the individual wheels and the ground are normally referred to as cornering forces. According to Ackermann, et al. (2002, equation (6.4.1)), the cornering forces are functions of the sideslip angles. They state that the relationship between the lateral force and the wheel slip angle, when the camber angle of the wheel is zero and when no sliding is taking place, is given as:

$$F_{yi} = \mu_i C_{\alpha i} \alpha_i \cos \delta_i \quad \text{where} \quad i = 1, 2, 3, 4 \qquad \text{[3.28]}$$

3.6   *Linearized model*

Most equations derived so far are nonlinear due to the presence of trigonometrical functions. Nonlinearity is also coming from the fact that naturally wheel forces are not linear. Ackermann et al. (2002) say that in normal driving situations (except slow parking manoeuvres), the most important nonlinearity is the uncertain wheel model. If small angles are assumed, like if we assume small steering angles, small sideslip angles of the wheels and small sideslip angle of the vehicle, we know that $\tan \theta = \sin \theta = \theta$ and $\cos \theta = 1$ where θ stands for a small angle.

3.6.1   *Linearized wheel sideslip angles*

According to You et al. (1998), if small angles are assumed, $|v_x| >> t|r|$. Therefore $v_x + tr \approx v_x$ and $v_x - tr \approx v_x$. Also $v \approx v_x$

From equation [3.24] to [3.27], the linearized wheel sideslip angles' equations are:

$$\alpha_i = \delta_i - \left(\frac{v\beta + ar}{v_x \pm tr} \right) \approx \delta_i - \left(\frac{v\beta + ar}{v_x} \right) \approx \delta_i - \left(\beta + \frac{ar}{v} \right) \text{ where } i = 1, 2 \qquad \text{[3.29]}$$

$$\alpha_i = \delta_i - \left(\frac{v\beta - l_r r}{v_x \pm tr} \right) \approx \delta_i - \left(\frac{v\beta - l_r r}{v_x} \right) \approx \delta_i - \left(\beta - \frac{l_r r}{v} \right) \text{ where } i = 3, 4 \qquad \text{[3.30]}$$

3.6.2 Linearized cornering and lateral forces

The second equation in equation [3.18] deals with the longitudinal acceleration of the vehicle. The analysis may be limited to the case where the vehicle is driven at a constant speed, which firstly means some propulsive force is necessary in the x direction to balance the effect of the aerodynamic drag force, and secondly that this equation need not be further considered. Turning to the first equation in equation [3.18], the resultant x-direction force $\sum F_{xi} - F_{dx}$, if not zero, would be very small and the multiplication of this small quantity with the sine of the small sideslip angle β can be ignored. Therefore, the linearized form of the first equation in equation [3.18] reduces to:

$$mv\left(\dot{\beta}+r\right) = F_{y1} + F_{y2} + F_{y3} + F_{y4} + F_{d_y} \qquad [3.31]$$

From equation [3.28], it follows that the linearized lateral forces in the vehicle axis system, based on the assumption that δ_i is small, are:

$$F_{yi} = \mu_i C_{\alpha i}\alpha_i = \mu_i\left[C_{\alpha i}\delta_i - C_{\alpha i}\left(\beta + \frac{ar}{v}\right)\right] \quad \text{where} \quad i = 1,2 \qquad [3.32]$$

$$F_{yi} = \mu_i C_{\alpha i}\alpha_i = \mu_i\left[C_{\alpha i}\delta_i - C_{\alpha i}\left(\beta - \frac{l_r r}{v}\right)\right] \quad \text{where} \quad i = 3,4 \qquad [3.33]$$

3.6.3 Linearized yaw moments

The vehicle x-direction forces can be ignored based on the argument that they are quite small, and are also multiplied with a moment arm t which is typically half the length of the moment arms a and l_r of the lateral forces. Then the yaw motion equation reduces to:

$$I_z\dot{r} = aF_{y1} + aF_{y2} - l_r F_{y3} - l_r F_{y4} + F_{dy}l_{gp} + M_D \qquad [3.34]$$

3.6.4 Linearized equation of motion

The final linearized equations of motion will now be equations [3.31] and [3.34], which can now be summarised in matrix form as:

$$\begin{bmatrix} mv(\dot{\beta}+r) \\ I_z\dot{r} \end{bmatrix} = \begin{bmatrix} F_{y1} + F_{y2} + F_{y3} + F_{y4} + F_{d_y} \\ aF_{y1} + aF_{y2} - l_rF_{y3} - l_rF_{y4} + F_{dy}l_{gp} + M_D \end{bmatrix} \qquad [3.35]$$

Using equations [3.32] and [3.33] of the relationships between lateral forces and wheel slip angles, we have:

$$\dot{\beta} = \frac{1}{mv}[\mu_1 C_{\alpha1}\delta_1 - \mu_1 C_{\alpha1}\left(\beta + \frac{ar}{v}\right) + \mu_2 C_{\alpha2}\delta_2 - \mu_2 C_{\alpha2}\left(\beta + \frac{ar}{v}\right)$$

$$+ \mu_3 C_{\alpha3}\delta_3 - \mu_3 C_{\alpha3}\left(\beta - \frac{l_r r}{v}\right) + \mu_4 C_{\alpha4}\delta_4 - \mu_4 C_{\alpha4}\left(\beta - \frac{l_r r}{v}\right) + F_{d_y}] - r$$

$$\dot{r} = \frac{1}{I_z}[a\mu_1 C_{\alpha1}\delta_1 - a\mu_1 C_{\alpha1}\left(\beta + \frac{ar}{v}\right) + a\mu_2 C_{\alpha2}\delta_2 - a\mu_2 C_{\alpha2}\left(\beta + \frac{ar}{v}\right)$$

$$- \mu_3 l_r C_{\alpha3}\delta_3 + \mu_3 l_r C_{\alpha3}\left(\beta - \frac{l_r r}{v}\right) - \mu_4 l_r C_{\alpha4}\delta_4 + \mu_4 l_r C_{\alpha4}\left(\beta - \frac{l_r r}{v}\right) + F_{dy}l_{gp} + M_D]$$

$$[3.36]$$

In matrix form:

$$\begin{bmatrix} \dot{\beta} \\ \dot{r} \end{bmatrix} = \begin{bmatrix} C_1 & C_2 \\ C_3 & C_4 \end{bmatrix}\begin{bmatrix} \beta \\ r \end{bmatrix} + \begin{bmatrix} \dfrac{\mu_1 C_{\alpha1}}{mv} & \dfrac{\mu_2 C_{\alpha2}}{mv} & \dfrac{\mu_3 C_{\alpha3}}{mv} & \dfrac{\mu_4 C_{\alpha4}}{mv} \\ \dfrac{a\mu_1 C_{\alpha1}}{I_z} & \dfrac{a\mu_2 C_{\alpha2}}{I_z} & -\dfrac{\mu_3 l_r C_{\alpha3}}{I_z} & -\dfrac{\mu_4 l_r C_{\alpha4}}{I_z} \end{bmatrix}\begin{bmatrix} \delta_1 \\ \delta_2 \\ \delta_3 \\ \delta_4 \end{bmatrix} + \begin{bmatrix} \dfrac{1}{mv} & 0 \\ \dfrac{l_{gp}}{I_z} & \dfrac{1}{I_z} \end{bmatrix}\begin{bmatrix} F_{d_y} \\ M_D \end{bmatrix}$$

$$[3.37]$$

Where:

$$C_1 = -\frac{1}{mv}\left(\mu_1 C_{\alpha1} + \mu_2 C_{\alpha2} + \mu_3 C_{\alpha3} + \mu_4 C_{\alpha4}\right) \qquad [3.38]$$

$$C_2 = \frac{1}{mv^2}\left(-a\mu_1 C_{\alpha 1} - a\mu_2 C_{\alpha 2} + l_r \mu_3 C_{\alpha 3} + l_r \mu_4 C_{\alpha 4}\right) - 1 \qquad [3.39]$$

$$C_3 = \frac{1}{I_z}\left(-a\mu_1 C_{\alpha 1} - a\mu_2 C_{\alpha 2} + l_r \mu_3 C_{\alpha 3} + l_r \mu_4 C_{\alpha 4}\right) \qquad [3.40]$$

$$C_4 = \frac{1}{I_z v}\left(-a^2 \mu_1 C_{\alpha 1} - a^2 \mu_2 C_{\alpha 2} - l_r^{\,2} \mu_3 C_{\alpha 3} - l_r^{\,2} \mu_4 C_{\alpha 4}\right) \qquad [3.41]$$

i.e. this is in the form of a state space equation and using Friedland (1986) notations, equation [3.37] can be written as:

$$\dot{x} = Ax + Bu + Ex_d \quad \text{and} \qquad [3.42]$$

$$\dot{y} = Cx + Du \qquad [3.43]$$

Where

$$A = \begin{bmatrix} C_1 & C_2 \\ C_3 & C_4 \end{bmatrix} \qquad\qquad B = \begin{bmatrix} \dfrac{\mu_1 C_{\alpha 1}}{mv} & \dfrac{\mu_2 C_{\alpha 2}}{mv} & \dfrac{\mu_3 C_{\alpha 3}}{mv} & \dfrac{\mu_4 C_{\alpha 4}}{mv} \\[2ex] \dfrac{a\mu_1 C_{\alpha 1}}{I_z} & \dfrac{a\mu_2 C_{\alpha 2}}{I_z} & -\dfrac{\mu_3 l_r C_{\alpha 3}}{I_z} & -\dfrac{\mu_4 l_r C_{\alpha 4}}{I_z} \end{bmatrix}$$

$$E = \begin{bmatrix} \dfrac{1}{mv} & 0 \\[2ex] \dfrac{l_{gp}}{I_z} & \dfrac{1}{I_z} \end{bmatrix} \qquad\qquad x = \begin{bmatrix} \beta \\ r \end{bmatrix}$$

$$u = \begin{bmatrix} \delta_1 \\ \delta_2 \\ \delta_3 \\ \delta_4 \end{bmatrix} \qquad\qquad x_d = \begin{bmatrix} F_{d_y} \\ M_D \end{bmatrix} \qquad [3.44]$$

The output from this linearized model, given by equation [3.43], is the vector of lateral acceleration at the decoupling point and yaw rate as shown later.

21

3.7   *Robust controller*

Ackermann et al. (2002 pp. 177,178) suggested the implementation of a robust controller to aid the driver in his steering task and this section is essentially based on their suggestions. To begin with, they explain that there exist a point called a decoupling point, as shown in Figure 3-3, which experiences a lateral acceleration a_{yDP}. This position is used to decouple two steering tasks of the vehicle, which are path tracking by the driver and the automatically controlled yaw stabilization and disturbance compensation. Ackermann et al. (2002), further explain that the indirect influence of the disturbance torques on the lateral acceleration a_{yDP} via the vehicle dynamics should be compensated such that the driver controls the undisturbed a_{yDP} in his or her path tracking task. They pointed out that in system theoretical terms, the task separation requires the yaw rate r to be non-observable from a_{yDP}. The condition for this decoupling is that $l_{DP} = I_z / ml_r$. This may be shown as follows, with reference to figure 3-3:
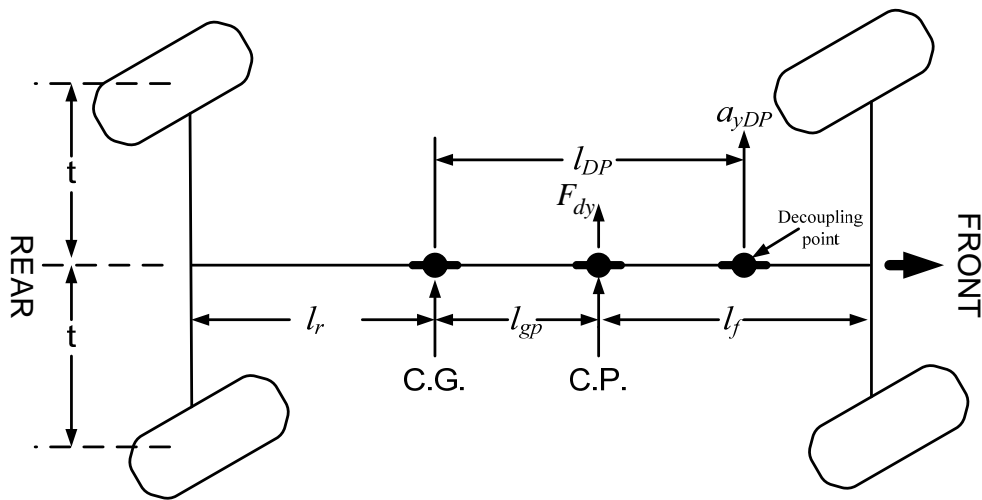

Figure 3-3:   **Decoupling point**

$$a_{yDP} = a_{yCG} + l_{DP} \frac{\partial r}{\partial t}$$

$$ma_{yCG} = F_{y1} + F_{y2} + F_{y3} + F_{y4} + F_{dy}$$

$$I_z \frac{\partial r}{\partial t} = \left(F_{y1} + F_{y2}\right)\left(l_f + l_{gp}\right) - \left(F_{y3} + F_{y4}\right)l_r + F_{dy}l_{gp} + M_D$$

$$a_{yDP} = \frac{\left(F_{y1} + F_{y2}\right)}{m} + \frac{\left(F_{y1} + F_{y2}\right)\left(l_f + l_{gp}\right)l_{DP}}{I_z} + \frac{\left(F_{y3} + F_{y4}\right)}{m} - \frac{\left(F_{y3} + F_{y4}\right)l_r l_{DP}}{I_z}$$
$$+ M_D \frac{l_{DP}}{I_z} + \frac{F_{dy}l_{gp}l_{DP}}{I_z} + \frac{F_{dy}}{m}$$

[3.45]

By defining the decoupling point such that

$$l_{DP} = I_z / ml_r$$ [3.46]

the contribution of the lateral forces at the rear wheels to the acceleration of the

decoupling point is zero, so that

$$a_{yDP} = \frac{\left(F_{y1} + F_{y2}\right)}{m} + \frac{\left(F_{y1} + F_{y2}\right)\left(l_f + l_{gp}\right).l_{DP}}{I_z} + M_D \frac{l_{DP}}{I_z} + \frac{F_{dy}l_{gp}l_{DP}}{I_z} + \frac{F_{dy}}{m}$$

$$= \left(F_{y1} + F_{y2}\right)\left[\frac{1}{m} + \frac{\left(l_f + l_{gp}\right)}{ml_r}\right] + \frac{M_D}{ml_r} + \frac{F_{dy}l_{gp}}{ml_r} + \frac{F_{dy}}{m}$$

$$= \frac{1}{m}\left(F_{y1} + F_{y2}\right)\left[1 + \frac{l_f + l_{gp}}{l_r}\right] + \frac{M_D}{ml_r} + \frac{F_{dy}l_{gp}}{ml_r} + \frac{F_{dy}}{m}$$

$$a_{yDP} = \frac{1}{ml_r}\left(F_{y1} + F_{y2}\right)l + \frac{M_D}{ml_r} + \frac{F_{dy}l_{gp}}{ml_r} + \frac{F_{dy}}{m}$$ [3.47]

Hence

$$a_{yDP} = \left[\sum_{i=1}^{2} F_{yi}l + M_D + F_{dy}\left(l_r + l_{gp}\right)\right] \bigg/ ml_r$$ [3.48]

$$= \left[\sum_{i=1}^{2} \mu_i C_{\alpha i} \left(\delta_i - \beta - ar/v \right) l + M_D + F_{dy} \left(l_r + l_{gp} \right) \right] \Big/ ml_r \qquad [3.49]$$

Ackermann at al. (2002), stress that this unilateral decoupling must be robust for all operating conditions. The feedback control law used to make the yaw rate r non-observable from the lateral acceleration a_{yDP} at the decoupling point, as suggested by these authors (Ackermann at al. 2002, p. 186), is:

$$\frac{\partial \delta_c}{\partial t} = r_{ref} - \left[r + \frac{l_{DP} - a}{v} \dot{r} \right] \qquad [3.50]$$

Making I_z in equation [3.46] subject of formula and substituting this relationship into equation [3.35], we have:

$$\begin{bmatrix} mv\left(\dfrac{\partial \beta}{\partial t} + r \right) \\[2ex] ml_r l_{DP} \dfrac{\partial r}{\partial t} \end{bmatrix} = \begin{bmatrix} F_{y1} + F_{y2} + F_{y3} + F_{y4} + F_{d_y} \\[1ex] aF_{y1} + aF_{y2} - l_r F_{y3} - l_r F_{y4} + F_{dy} l_{gp} + M_D \end{bmatrix} \qquad [3.51]$$

Solving equation [3.51] by first multiplying the top equation by l_r and then adding the two equations, followed by multiplying the top equation by a and then subtracting the bottom equation from the top equation, results in the following two simultaneous equations:

$$ml_r \left[v\left(\frac{\partial \beta}{\partial t} + r \right) + l_{DP} \frac{\partial r}{\partial t} \right] = F_{y1}l + F_{y2}l + F_{dy}l_r + F_{dy}l_{gp} + M_D \qquad [3.52]$$

$$m \left[va\left(\frac{\partial \beta}{\partial t} + r \right) - l_r l_{DP} \frac{\partial r}{\partial t} \right] = F_{y3}l + F_{y4}l + F_{dy}a - F_{dy}l_{gp} - M_D \qquad [3.53]$$

Substituting for *r* from equation [3.50]

$$r = r_{ref} - \frac{\partial \delta_c}{\partial t} - \left(l_{DP} - a \right) \frac{\partial r}{\partial t} \Big/ v \qquad [3.54]$$

into equation [3.52], the result is

$$mvl_r \left[\frac{\partial \beta}{\partial t} - \frac{\partial \delta_c}{\partial t} + a \frac{\partial r}{\partial t} \middle/ v \right] = F_{y1}l + F_{y2}l + F_{dy}l_r + F_{dy}l_{gp} + M_D - mvl_r r_{ref} \quad [3.55]$$

The linearization that renders equations [3.29] and [3.30] from equations [3.24] to [3.27] also implies that, after linearization, $\beta_1 = \beta_2$ and $\beta_3 = \beta_4$. Also, because the control law enforces $\delta_{c1} = \delta_{c2} = \delta_c$, there are no longer two distinctive γ angles after linearization i.e., $\gamma_{f1} = \gamma_{f2}$. Therefore, from now onwards, whenever the linearized model is discussed or used β_f will be used for both β_1 and β_2, β_r will be used for both β_3 and β_4, and γ_f for both γ_{f1} and γ_{f2}.

From $\gamma_f = \beta_f - \delta_c$ and substituting $\beta_f = \beta + ar/v$ from front wheels equation(see equation [3.29]), we have

$\gamma_f = \beta + ar/v - \delta_c$, which will give $\dot{\gamma}_f$ equal to the expression in the square brackets of equation [3.55]. Substituting $\dot{\gamma}_f$ for this expression leads to:

$$\frac{\partial \gamma_f}{\partial t} = \left[F_{y1}l + F_{y2}l + F_{dy}\left(l_r + l_{gp} \right) + M_D \right] \middle/ mvl_r - r_{ref} \quad [3.56]$$

Also from equation [3.48], it can be seen that:

$$a_{yDP} = v \left[\frac{\partial \gamma_f}{\partial t} + r_{ref} \right] \quad [3.57]$$

It can be noted from equation [3.56] that this first order equation in γ does not depend on the state variable r. This shows that the control law, equation [3.50], makes the yaw rate non-observable from the lateral acceleration a_{yDP} at the decoupling point. The lateral

forces are functions of slip angles i.e. $F_{y1} = F_{y1}(\alpha_1)$ and $F_{y2} = F_{y2}(\alpha_2)$. From figure 3-2,

$\alpha_1 = \delta_s - \gamma_f$ and thus independent of r. Therefore $F_{y1}(\delta_s - \gamma_f) = F_{y2}(\delta_s - \gamma_f)$. This

leads equation [3.56] to:

$$\frac{\partial \gamma_f}{\partial t} = \left[F_{y1}(\delta_s - \gamma_f)l + F_{y2}(\delta_s - \gamma_f)l + F_{dy}(l_r + l_{gp}) + M_D \right] \Big/ mvl_r - r_{ref}$$

[3.58]

3.8   *The decoupled yaw subsystem*

From the linearization that produces equation [3.30] from equations [3.26] and [3.27]

(see also the introduction of β_r just after equation [3.55]), we can see that:

$$\beta_r = \beta - l_r r / v$$

[3.59]

Therefore

$$\dot{\beta}_r = \dot{\beta} - l_r \dot{r} / v$$

Substituting for $\dot{\beta}$ from equation [3.53], we have:

$$\dot{\beta}_r = \frac{1}{mva} \left[lF_{y3} + lF_{y4} + F_{dy}(a - l_{gp}) - M_D \right] + \frac{l_r(l_{DP} - a)}{va} \dot{r} - r$$

[3.60]

Solving for $\dfrac{\partial r}{\partial t}$ from second row of equation [3.51], we have:

$$\frac{\partial r}{\partial t} = \frac{1}{ml_r l_{DP}} \left[aF_{y1} + aF_{y2} - l_r F_{y3} - l_r F_{y4} + F_{dy} l_{gp} + M_D \right]$$

[3.61]

From equation [3.48], we have

$$\sum_{i=1}^{2} F_{yi} = \left[a_{yDP} ml_r - M_D - F_{dy}(l_r + l_{gp}) \right] \Big/ l$$

[3.62]

When equation [3.62] is substituted into equation [3.61], we have:

$$\frac{\partial r}{\partial t} = \frac{1}{ml_r l_{DP}}\left[a\left[a_{yDP}ml_r - M_D - F_{dy}\left(l_r + l_{gp}\right)\right]\Big/ l - l_r F_{y3} - l_r F_{y4} + F_{dy}l_{gp} + M_D\right]$$

$$\frac{\partial r}{\partial t} = \frac{aa_{yDP}}{ll_{DP}} - \frac{aM_D}{ml_r l_{DP}l} - \frac{aF_{dy}\left(l_r + l_{gp}\right)}{ml_r l_{DP}l} - \frac{F_{y3} + F_{y4}}{ml_{DP}} + \frac{F_{dy}l_{gp}}{ml_r l_{DP}} + \frac{M_D}{ml_r l_{DP}}$$

$$\frac{\partial r}{\partial t} = \frac{aa_{yDP}}{ll_{DP}} - \frac{F_{y3} + F_{y4}}{ml_{DP}} + \frac{F_{dy}}{ml_r l_{DP}}\left[l_{gp} - \frac{a\left(l_r + l_{gp}\right)}{l}\right] + \frac{M_D}{ml_r l_{DP}}\left(1 - \frac{a}{l}\right)$$

$$\frac{\partial r}{\partial t} = \frac{aa_{yDP}}{ll_{DP}} - \frac{F_{y3} + F_{y4}}{ml_{DP}} - \frac{F_{dy}l_f}{mll_{DP}} + \frac{M_D}{mll_{DP}} \qquad\qquad [3.63]$$

where $l = \left(l_r + l_{gp} + l_f\right)$ and $l - a = l_r$

Substituting equation [3.63] into equation [3.60] will yield the following yaw subsystem equation in state space form.

$$\begin{bmatrix} \dot{\beta}_r \\ \dot{r} \end{bmatrix} = \frac{1}{ml_{DP}}\begin{bmatrix} (l_{DP} + l_r)/v \\ -1 \end{bmatrix}\left[\sum_{i=3}^{4}F_{yi} - M_D/l\right]$$
$$+ \begin{bmatrix} \frac{1}{va}\left[ll_{DP}a - ll_{DP}l_{gp} - l_r l_{DP}l_f + l_r l_f a\right] \\ -l_f \end{bmatrix}\frac{F_{dy}}{mll_{DP}}$$
$$- \begin{bmatrix} 1 \\ 0 \end{bmatrix}r + \begin{bmatrix} l_r(l_{DP} - a)/v \\ a \end{bmatrix}\frac{a_{yDP}}{ll_{DP}}$$

$$\begin{bmatrix} \dot{\beta}_r \\ \dot{r} \end{bmatrix} = \frac{1}{ml_{DP}}\begin{bmatrix} (l_{DP} + l_r)/v \\ -1 \end{bmatrix}\left[\sum_{i=3}^{4}F_{yi} - M_D/l\right]$$
$$+ \begin{bmatrix} \frac{\rho_{F_1}}{va} \\ -l_f \end{bmatrix}\frac{F_{dy}}{mll_{DP}} - \begin{bmatrix} 1 \\ 0 \end{bmatrix}r + \begin{bmatrix} l_r(l_{DP} - a)/v \\ a \end{bmatrix}\frac{a_{yDP}}{ll_{DP}} \qquad [3.64]$$

Where $\rho_{F_1} = \left[ll_{DP}a - ll_{DP}l_{gp} - l_r l_{DP}l_f + l_r l_f a\right]$

Equation [3.64] is similar to what Ackermann et. al (2002) found with few additionals in the terms of aerodynamics forces F_{dy} and distance terms. The quantity a_{yDP} is used as the coupling term as it may be measured with accelerometers. a_{yDP} is also used in the task separation.

3.9   *Transfer functions*

This section discusses the transfer functions of the two systems which are the vehicle that does not have any controlling measures and the vehicle with controlling measures. We will begin our discussions with an uncontrolled vehicle system and later on we will talk about a controlled vehicle system.

3.9.1   *Uncontrolled vehicle system*

From equation [3.37] the characteristic polynomial would be:

$$P(s) = (s - C_1)(s - C_4) - C_2 C_3 \tag{3.65}$$

$$= s^2 + c_1 s + c_2 \text{ where} \tag{3.66}$$

$$c_1 = -(C_4 + C_1)$$

$$c_2 = C_1 C_4 - C_2 C_3$$

Also, the resolvent is given by:

$$(s\mathbf{I} - \mathbf{A})^{-1} = \frac{1}{P(s)} \begin{bmatrix} s - C_4 & C_2 \\ C_3 & s - C_1 \end{bmatrix} \tag{3.67}$$

The uncontrolled (undecoupled) transfer functions will now be derived.

Equation [3.37] may also be written as:

$$\begin{bmatrix} \dot{\beta} \\ \dot{r} \end{bmatrix} = \begin{bmatrix} C_1 & C_2 \\ C_3 & C_4 \end{bmatrix} \begin{bmatrix} \beta \\ r \end{bmatrix} + \begin{bmatrix} \dfrac{\mu_1 C_{\alpha 1}}{mv} & \dfrac{\mu_2 C_{\alpha 2}}{mv} & \dfrac{\mu_3 C_{\alpha 3}}{mv} & \dfrac{\mu_4 C_{\alpha 4}}{mv} & \dfrac{1}{mv} & 0 \\ \dfrac{a\mu_1 C_{\alpha 1}}{I_z} & \dfrac{a\mu_2 C_{\alpha 2}}{I_z} & -\dfrac{l_r \mu_3 C_{\alpha 3}}{I_z} & -\dfrac{l_r \mu_4 C_{\alpha 4}}{I_z} & \dfrac{l_{gp}}{I_z} & \dfrac{1}{I_z} \end{bmatrix} \begin{bmatrix} \delta_1 \\ \delta_2 \\ \delta_3 \\ \delta_4 \\ F_{d_y} \\ M_D \end{bmatrix}$$

[3.68]

Which is in the standard form

$$\dot{x} = Ax + Bu$$ [3.69]

Where the state vector x and matrix A are defined as in equation [3.44], and

$$B = \begin{bmatrix} \dfrac{\mu_1 C_{\alpha 1}}{mv} & \dfrac{\mu_2 C_{\alpha 2}}{mv} & \dfrac{\mu_3 C_{\alpha 3}}{mv} & \dfrac{\mu_4 C_{\alpha 4}}{mv} & \dfrac{1}{mv} & 0 \\ \dfrac{a\mu_1 C_{\alpha 1}}{I_z} & \dfrac{a\mu_2 C_{\alpha 2}}{I_z} & -\dfrac{l_r \mu_3 C_{\alpha 3}}{I_z} & -\dfrac{l_r \mu_4 C_{\alpha 4}}{I_z} & \dfrac{l_{gp}}{I_z} & \dfrac{1}{I_z} \end{bmatrix} \text{ and}$$

$$u = \begin{bmatrix} \delta_1 & \delta_2 & \delta_3 & \delta_4 & F_{dy} & M_D \end{bmatrix}^T$$

Let the output be r and a_{yDP} or

$$y = \begin{bmatrix} r \\ a_{yDP} \end{bmatrix}$$ [3.70]

Then the output equation is in the form:

$$y = Cx + Du$$

Using equation [3.49]

$$C = \begin{bmatrix} 0 & 1 \\ \dfrac{-l}{ml_r} \sum\limits_{i=1}^{2} \mu_i C_{\alpha i} & \dfrac{-al/v}{ml_r} \sum\limits_{i=1}^{2} \mu_i C_{\alpha i} \end{bmatrix} \text{ and}$$

29

$$D = \begin{bmatrix} 0 & 0 & 0 & 0 & 0 & 0 \\ \dfrac{\mu_1 l C_{\alpha 1}}{m l_r} & \dfrac{\mu_2 l C_{\alpha 2}}{m l_r} & 0 & 0 & \dfrac{l_r + l_{gp}}{m l_r} & \dfrac{1}{m l_r} \end{bmatrix}$$

The Laplace transformation of equation [3.69] is:

$$x(s)s = Ax(s) + Bu$$
$$(sI - A)x(s) = Bu \qquad\qquad [3.71]$$
$$x(s) = (sI - A)^{-1}Bu$$

Substituting equation [3.71] into the Laplace transformation of equation [3.70], we have:

$$y(s) = Cx(s) + Du$$
$$= C(sI - A)^{-1}Bu + Du \qquad\qquad [3.72]$$
$$= \left[C(sI - A)^{-1}B + D\right]u$$

This can be expressed in the following form:

$$\begin{bmatrix} r(s) \\ a_{yDP}(s) \end{bmatrix} = \frac{1}{P(s)}\begin{bmatrix} b_1 & b_2 & b_3 & b_4 & b_5 & b_6 \\ b_7 & b_8 & b_9 & b_{10} & b_{11} & b_{12} \end{bmatrix}\begin{bmatrix} \delta_1(s) \\ \delta_2(s) \\ \delta_3(s) \\ \delta_4(s) \\ F_{d_y}(s) \\ M_D(s) \end{bmatrix} + \begin{bmatrix} 0 & 0 \\ \dfrac{\mu_1 l C_{\alpha 1}}{m l_r} & \dfrac{\mu_2 l C_{\alpha 2}}{m l_r} \end{bmatrix}\begin{bmatrix} \delta_1(s) \\ \delta_2(s) \end{bmatrix}$$

$$+ \begin{bmatrix} 0 & 0 \\ \dfrac{lr + l_{gp}}{m l_r} & \dfrac{1}{m l_r} \end{bmatrix}\begin{bmatrix} F_{dy}(s) \\ M_D(s) \end{bmatrix} \qquad\qquad [3.73]$$

Where:

$$b_1 = \frac{C_3\mu_1 C_{\alpha 1}}{mv} + \frac{(s - C_1)a\mu_1 C_{\alpha 1}}{I_z}; \qquad\qquad b_2 = \frac{C_3\mu_2 C_{\alpha 2}}{mv} + \frac{(s - C_1)a\mu_2 C_{\alpha 2}}{I_z};$$

$$b_3 = \frac{C_3\mu_3 C_{\alpha 3}}{mv} - \frac{(s - C_1)l_r\mu_3 C_{\alpha 3}}{I_z}; \qquad\qquad b_4 = \frac{C_3\mu_4 C_{\alpha 4}}{mv} - \frac{(s - C_1)l_r\mu_4 C_{\alpha 4}}{I_z};$$

$$b_5 = \frac{C_3}{mv} + (s - C_1)\frac{l_{gp}}{I_z} ; \qquad b_6 = \frac{(s - C_1)}{I_z} ; \qquad b_7 = \mu_1 C_{\alpha1}\left(\frac{k_k}{mv} + \frac{aj_j}{I_z}\right) ;$$

$$b_8 = \mu_2 C_{\alpha2}\left(\frac{k_k}{mv} + \frac{aj_j}{I_z}\right) ; \qquad b_9 = \mu_3 C_{\alpha3}\left(\frac{k_k}{mv} - \frac{l_r j_j}{I_z}\right) ;$$

$$b_{10} = \mu_4 C_{\alpha4}\left(\frac{k_k}{mv} - \frac{l_r j_j}{I_z}\right) ; \qquad b_{11} = \left(\frac{k_k}{mv} + \frac{l_{gp} j_j}{I_z}\right) ; \qquad b_{12} = \frac{j_j}{I_z} ;$$

$$k_k = \frac{-l\sum \mu_i C_{\alpha i}}{ml_r}(s - C_4) - \frac{a/v\sum \mu_i C_{\alpha i}}{ml_r} C_3 \quad \text{and}$$

$$j_j = \frac{-l\sum \mu_i C_{\alpha i}}{ml_r} C_2 - \frac{a/v\sum \mu_i C_{\alpha i}}{ml_r}(s - C_1) \quad \text{where for both} \quad k_k \quad \text{and} \quad j_j, \text{the summation is}$$

for i from 1 to 2.

This can be reduced to:

$$P(s)\begin{bmatrix} r(s) \\ a_{yDP}(s) \end{bmatrix} = \begin{bmatrix} d_1 & d_2 & d_3 & d_4 & d_5 & d_6 \\ d_7 & d_8 & d_9 & d_{10} & d_{11} & d_{12} \end{bmatrix}\begin{bmatrix} \delta_1(s) \\ \delta_2(s) \\ \delta_3(s) \\ \delta_4(s) \\ F_{d_y}(s) \\ M_D(s) \end{bmatrix} \qquad [3.74]$$

Where d_1 to d_6 will be the same as b_1 to b_6 respectively and:

$$d_7 = b_7 + \frac{P(s)\mu_1 C_{\alpha1}}{ml_r} ; \qquad d_8 = b_8 + \frac{P(s)\mu_2 C_{\alpha2}}{ml_r} ; \qquad d_{11} = b_{11} + \frac{P(s)(l_r + l_{gp})}{ml_r}$$

and

$$d_{12} = b_{12} + \frac{P(s)}{ml_r} \quad \text{while} \quad d_9 \quad \text{and} \quad d_{10} \quad \text{will remain as} \quad b_9 \quad \text{and} \quad b_{10} \quad \text{respectively.}$$

3.9.2   Controlled vehicle system

From equation [3.58] we can substitute the linearized equivalent of

$F_{yi}\left(\delta_s - \gamma_f\right) = \mu_i C_{\alpha i}\left(\delta_s - \gamma_f\right)$ and the results are as shown below:

$$\frac{\partial \gamma_f}{\partial t} = \left[F_{y1}l + F_{y2}l + F_{dy}\left(l_r + l_{gp}\right) + M_D\right]\Big/ mvl_r - r_{ref}$$

$$\frac{\partial \gamma_f}{\partial t} = \left[l\sum_{i=1}^{2}\mu_i C_{\alpha i}\alpha_i + F_{dy}\left(l_r + l_{gp}\right) + M_D\right]\Big/ mvl_r - r_{ref}$$

$$\frac{\partial \gamma_f}{\partial t} = \left[\left(\mu_1 C_{\alpha 1} + \mu_2 C_{\alpha 2}\right)\left(\delta_s - \gamma_f\right)l + F_{dy}\left(l_r + l_{gp}\right) + M_D\right]\Big/ mvl_r - r_{ref} \quad [3.75]$$

From equation [3.57], we have

$$a_{yDP} = v\left(\frac{\partial \gamma_f}{\partial t} + r_{ref}\right)$$

$$= -\frac{l\gamma_f\left(\mu_1 C_{\alpha 1} + \mu_2 C_{\alpha 2}\right)}{ml_r} + \frac{l\delta_s\left(\mu_1 C_{\alpha 1} + \mu_2 C_{\alpha 2}\right)}{ml_r} + \frac{F_{dy}\left(l_r + l_{gp}\right)}{ml_r} + \frac{M_D}{ml_r}$$

$$[3.76]$$

Substituting equation [3.76] into equation [3.64] with the help of equations [3.33] and [3.59], we have:

$$\begin{bmatrix} \dot{\beta}_r \\ \dot{r} \end{bmatrix} = \begin{bmatrix} a_1 & -1 \\ a_2 & 0 \end{bmatrix}\begin{bmatrix} \beta_r \\ r \end{bmatrix} + \begin{bmatrix} a_3 \\ a_4 \end{bmatrix}\begin{bmatrix} \gamma_f \end{bmatrix} + \begin{bmatrix} a_5 & a_6 & a_7 & a_8 \\ a_9 & a_{10} & a_{11} & a_{12} \end{bmatrix}\begin{bmatrix} \delta_s \\ \delta_r \\ F_{dy} \\ M_D \end{bmatrix} \quad [3.77]$$

where for the time being, $\delta_3 = \delta_4 = \delta_r$. Later on, in section 4.2.3.1, the concept of independent steering angles on both front and rear wheels is re-introduced.

$$a_1 = -\frac{(l_{DP}+l_r)}{mvl_{DP}}\sum_{i=3}^{4}\mu_i C_{\alpha i}\;;\qquad a_2 = \frac{1}{ml_{DP}}\sum_{i=3}^{4}\mu_i C_{\alpha i}\;;\qquad a_3 = -\frac{(l_{DP}-a)}{mvl_{DP}}\sum_{i=1}^{2}\mu_i C_{\alpha i}$$

$$a_4 = -\frac{a}{ml_r l_{DP}}\sum_{i=1}^{2}\mu_i C_{\alpha i}\;;\qquad a_5 = \frac{(l_{DP}-a)}{mvl_{DP}}\sum_{i=1}^{2}\mu_i C_{\alpha i}\;;\qquad a_6 = \frac{(l_{DP}+l_r)}{mvl_{DP}}\sum_{i=3}^{4}\mu_i C_{\alpha i}\;;$$

$$a_7 = \frac{a\rho_{F_2}+\rho_{F_1}}{mvall_{DP}}\;;\qquad a_8 = \frac{1}{mvl_{DP}}\;;\qquad a_9 = \frac{a}{ml_r l_{DP}}\sum_{i=1}^{2}\mu_i C_{\alpha i}\;;$$

$$a_{10} = -\frac{1}{ml_{DP}}\sum_{i=3}^{4}\mu_i C_{\alpha i}\;;\qquad a_{11} = \frac{l_{gp}}{ml_{DP}l_r}\qquad a_{12} = \frac{1}{ml_r l_{DP}}\;;$$

Where $\rho_{F_2} = (l_{DP}-a)(l_r+l_{gp})$

The above state space equation of the robustly decoupled vehicle, equation [3.77], together with equation [3.75], can be grouped into:

$$\begin{bmatrix}\dot{\beta}_r\\ \dot{r}\\ \dot{\gamma}_f\end{bmatrix} = \begin{bmatrix}a_1 & -1 & a_3\\ a_2 & 0 & a_4\\ 0 & 0 & a_{13}\end{bmatrix}\begin{bmatrix}\beta_r\\ r\\ \gamma_f\end{bmatrix} + \begin{bmatrix}a_5 & a_6 & a_7 & a_8 & 0\\ a_9 & a_{10} & a_{11} & a_{12} & 0\\ a_{14} & 0 & a_{15} & a_{16} & -1\end{bmatrix}\begin{bmatrix}\delta_s\\ \delta_r\\ F_{dy}\\ M_D\\ r_{ref}\end{bmatrix}\qquad [3.78]$$

Where:

$$a_{13} = -\frac{l}{mvl_r}\sum_{i=1}^{2}\mu_i C_{\alpha i}\;;\qquad a_{14} = \frac{l}{mvl_r}\sum_{i=1}^{2}\mu_i C_{\alpha i}\;;$$

$$a_{15} = \frac{l_r+l_{gp}}{mvl_r}\;;\qquad a_{16} = \frac{1}{mvl_r}\;;$$

The decoupled output equation is:

$$\begin{bmatrix} r \\ a_{yDP} \end{bmatrix} = \begin{bmatrix} 0 & 1 & 0 \\ 0 & 0 & f_1 \end{bmatrix} \begin{bmatrix} \beta_r \\ r \\ \gamma_f \end{bmatrix} + \begin{bmatrix} 0 & 0 & 0 & 0 & 0 \\ f_2 & 0 & f_3 & f_4 & 0 \end{bmatrix} \begin{bmatrix} \delta_s \\ \delta_r \\ F_{dy} \\ M_D \\ r_{ref} \end{bmatrix} \qquad [3.79]$$

where:

$$f_1 = -\frac{l}{ml_r} \sum_{i=1}^{2} \mu_i C_{\alpha i} ; \qquad f_2 = \frac{l}{ml_r} \sum_{i=1}^{2} \mu_i C_{\alpha i} ; \qquad f_3 = \frac{\left(l_r + l_{gp}\right)}{ml_r} ; \qquad f_4 = \frac{1}{ml_r} ;$$

Equations [3.78] and [3.79] are recognised as a 3rd order state space model of the decoupled controlled system, of a form similar to equations [3.68] and [3.70], with state vector $\begin{bmatrix} \beta_r & r & \gamma_f \end{bmatrix}^T$, input vector $\begin{bmatrix} \delta_s & \delta_r & F_{dy} & M_D & r_{ref} \end{bmatrix}^T$ i.e., the vector on the far right of equation [3.79]), the output vector $\begin{bmatrix} r & a_{yDP} \end{bmatrix}^T$ and the matrices given by:

$$A = \begin{bmatrix} a_1 & -1 & a_3 \\ a_2 & 0 & a_4 \\ 0 & 0 & a_{13} \end{bmatrix}$$

$$B = \begin{bmatrix} a_5 & a_6 & a_7 & a_8 & 0 \\ a_9 & a_{10} & a_{11} & a_{12} & 0 \\ a_{14} & 0 & a_{15} & a_{16} & -1 \end{bmatrix}$$

$$C = \begin{bmatrix} 0 & 1 & 0 \\ 0 & 0 & f_1 \end{bmatrix}$$

$$D = \begin{bmatrix} 0 & 0 & 0 & 0 & 0 \\ f_2 & 0 & f_3 & f_4 & 0 \end{bmatrix}$$

Transforming equations [3.78] and [3.79] to the Laplace domain leads to the transfer functions g_1 to g_9, defined by:

$$
\begin{bmatrix} r \\ a_{yDP} \end{bmatrix} = \begin{bmatrix} g_1 & g_2 & g_3 & g_4 & g_5 \\ g_6 & 0 & g_7 & g_8 & g_9 \end{bmatrix} \begin{bmatrix} \delta_s \\ \delta_r \\ F_{dy} \\ M_D \\ r_{ref} \end{bmatrix}
$$

[3.80]

Where:

$$
g_1 = \frac{s\left(\mu_1 C_{\alpha 1} + \mu_2 C_{\alpha 2}\right) v\left(amvs + q\right)}{\left(mvl_r s + \mu_1 lC_{\alpha 1} + \mu_2 lC_{\alpha 2}\right)\left(mvl_{DP} s^2 + ps + z\right)}
$$

$$
g_2 = \frac{a_{10}\, s + \left(a_2\, a_6 - a_{10}\, a_1\right)}{s^2 - a_1\, s + a_2}
$$

$$
g_3 = \frac{a_{11}\, s^2 + \left(a_{15}\, a_4 + a_2\, a_7 - a_{11}\, a_{13} - a_{11}\, a_1\right) s + \left(a_{15}\, a_3\, a_2 - a_{15}\, a_4\, a_1 - a_2\, a_7\, a_{13} + a_{11}\, a_1\, a_{13}\right)}{s^3 - \left(a_{13} + a_1\right) s^2 + \left(a_1\, a_{13} + a_2\right) s - a_2\, a_{13}}
$$

$$
g_4 = \frac{a_{12}\, s^2 + \left(a_{16}\, a_4 + a_2\, a_8 - a_{12}\, a_{13} - a_{12}\, a_1\right) s + \left(a_{16}\, a_3\, a_2 - a_{16}\, a_4\, a_1 - a_2\, a_8\, a_{13} + a_{12}\, a_1\, a_{13}\right)}{s^3 - \left(a_{13} + a_1\right) s^2 + \left(a_1\, a_{13} + a_2\right) s - a_2\, a_{13}}
$$

$$
g_5 = \frac{\left(\mu_1 C_{\alpha 1} + \mu_2 C_{\alpha 2}\right) v\left(amvs + q\right)}{\left(mvl_r s + \mu_1 lC_{\alpha 1} + \mu_2 lC_{\alpha 2}\right)\left(mvl_{DP} s^2 + ps + z\right)}
$$

$$
g_6 = \frac{\left(\mu_1 v C_{\alpha 1} + \mu_2 v C_{\alpha 2}\right) s}{smvl_r + \left(\mu_1 lC_{\alpha 1} + \mu_2 lC_{\alpha 2}\right)}
$$

$$
g_7 = \frac{-\mu_1 C_{\alpha 1} l_r - \mu_1 C_{\alpha 1} l_{gp} - \mu_2 C_{\alpha 2} l_r - \mu_2 C_{\alpha 2} l_{gp} + smvl_r^2 + l_r \mu_2 lC_{\alpha 1} + l_r \mu_2 lC_{\alpha 2}}{\left(smvl_r + \mu_1 lC_{\alpha 1} + \mu_2 lC_{\alpha 2}\right) ml_r}
$$

$$
g_8 = \frac{-\mu_1 C_{\alpha 1} - \mu_2 C_{\alpha 2} + smvl_r + \mu_1 lC_{\alpha 1} + \mu_2 lC_{\alpha 2}}{\left(smvl_r + \mu_1 lC_{\alpha 1} + \mu_2 lC_{\alpha 2}\right) ml_r}
$$

$$
g_9 = \frac{\left(\mu_1 C_{\alpha 1} + \mu_2 C_{\alpha 2}\right) v}{smvl_r + \left(\mu_1 lC_{\alpha 1} + \mu_2 lC_{\alpha 2}\right)} \quad \text{and}
$$

$$p = \left(\mu_3 \, l_{Dp} \, C_{\alpha 3} + \mu_4 \, l_{Dp} \, C_{\alpha 4} + \mu_3 \, l_r \, C_{\alpha 3} + \mu_4 \, l_r \, C_{\alpha 4} \right),$$

$$q = \left(a\mu_3 \, C_{\alpha 3} + a\mu_4 \, C_{\alpha 4} + \mu_3 \, l_r \, C_{\alpha 3} + \mu_4 \, l_r \, C_{\alpha 4} \right),$$

$$z = \left(\mu_3 \, C_{\alpha 3} + \mu_4 C_{\alpha 4} \right) v$$

Some of the *g*-functions are expressed in terms of the basic parameters to highlight further simplification, whereas others are expressed in terms of the a-coefficients of equations [3.77] and [3.78] for the sake of simplicity without which they looked clumsy.

Equation [3.80] can be rewritten as:

$$
\begin{bmatrix} r \\ a_{yDP} \end{bmatrix} = \begin{bmatrix} g_1 & g_2 & g_3 & g_4 \\ g_6 & 0 & g_7 & g_8 \end{bmatrix} \begin{bmatrix} \delta_s + \dfrac{r_{ref}}{s} \\ \delta_r \\ F_{dy} \\ M_D \end{bmatrix}
\qquad\qquad \text{[3.81]}
$$

3.10 *Position of centre of pressure*

Hanke et al. (2001) conducted research on analysis and control of vehicle dynamics under cross wind conditions. As already pointed out, the resultant crosswind effect is thought to act at the centre of pressure. Generally, determining the centre of pressure can be a very complicated procedure since the pressure distribution is bound to change around the object under varying conditions. The position of the centre of pressure also depends on the type of the vehicle body. Hanke et al. (2001) show that, usually, the position of centre of pressure lies in the front half of the vehicle between the front axle and centre of gravity. This is in line with the explanation given by Hucho (1987), which states that there exists a place M which is called the aerodynamic reference point. This point is located in the middle of the wheel base and the middle of the track. Since the location of

C.G. of the experimental vehicle is way beyond the centre of the vehicle, M was assumed to lie between C.G. and C.P. Eventually the equation for deriving the distance between C.P. and C.G. will be the same as given by Hanke (2001).
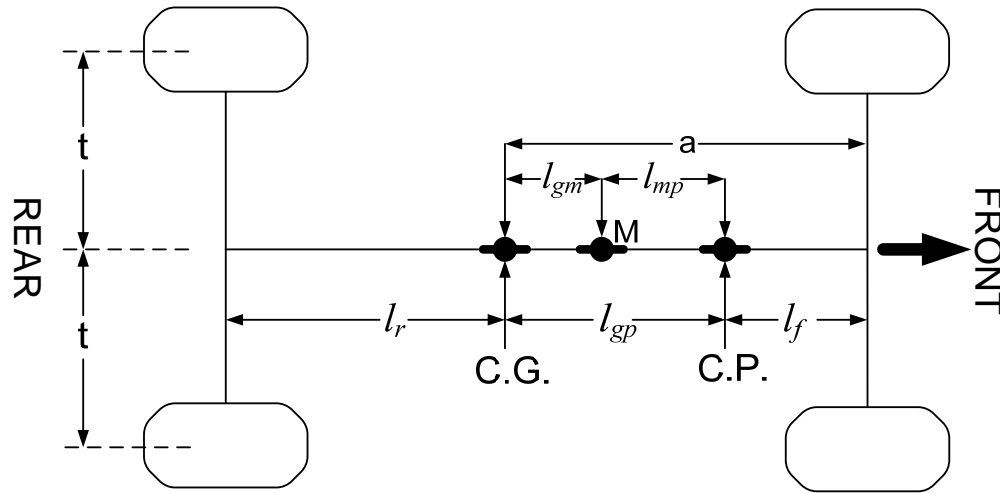

Figure 3-4:   **Location of centre of pressure**

$$l_{mp} = \frac{C_{Mz}}{C_{Fy}} l \qquad\qquad [3.82]$$

Then the equation between C.P. and C.G. can be found algebraically from:

$$l_{gp} = a - \frac{l}{2} + l_{mp} \text{, this gives}$$

$$l_{gp} = a - \frac{l}{2} + \frac{C_{Mz}}{C_{Fy}} l \qquad\qquad [3.83]$$

where these variables are as defined under nomenclature.

From the tables given in Gillespie (1992), the ratio of yaw moment coefficient to lateral force coefficient can be calculated to be approximately equal to 0.2.

i.e.

$$\frac{C_{Mz}}{C_{Fy}} \approx 0.2 \qquad\qquad\qquad\qquad\qquad\qquad\qquad\qquad [3.84]$$

3.11   *Conclusion*

This chapter was all about mathematical modelling of the experimental vehicle which

will be used in the simulations and experimental tests.

4   SIMULATIONS AND RESULTS

This section deals with the relationships between the input and output of the decoupled car system and conventional car system according to the equations derived in chapter 3. From the relationships that are derived, the equations are simulated and results are presented.

4.1   *Decoupled car*

The characteristic polynomial of the decoupled car is derived from equation [3.78] and can be written as:

$(s - a_{13})(s^2 - a_1 s + a_2)$ with meanings according to Ackermann et al. (2002, pp.207-208)

i.e.

$(s - a_{13})$ is the lateral characteristic polynomial and

$(s^2 - a_1 s + a_2)$ is the yaw characteristic polynomial.

The yaw characteristic polynomial will be written as:

$$P_{yaw} = (s^2 - a_1 s + a_2)$$

$$= s^2 \;+\; \frac{(l_{DP} + l_r)}{mvl_{DP}} \sum_{i=3}^{4} \mu_i C_{\alpha i} s \;+\; \frac{\sum_{i=3}^{4} \mu_i C_{\alpha i}}{ml_{DP}} \qquad [4.1]$$

In conventional second order way of writing equations, equation [4.1] can be written as:

$$P_{yaw} = s^2 + 2\zeta\omega_n s + \omega_n^2 \qquad [4.2]$$

with

$$\omega_n = \sqrt{\frac{\sum_{i=3}^{4} \mu_i C_{\alpha i}}{ml_{DP}}} \quad \text{and} \qquad [4.3]$$

$$\zeta = \frac{(l_{DP} + l_r)}{2v}\sqrt{\frac{\sum\limits_{i=3}^{4}\mu_i C_{\alpha i}}{ml_{DP}}} \qquad [4.4]$$

Equation [4.4] produces a small damping, this makes the yaw dynamics to oscillate. To have the meaningful results, the damping coefficient in the yaw dynamics equation has to be changed. According to Ackermann et al. (2004), the yaw dynamics can be stabilised by making ζ large.

For the decoupled car, the transfer functions will be, (see equation [3.81]):

$$G(s) = \frac{r(s)}{\delta_s(s)} = g_1 \qquad [4.5]$$

$$G_F(s) = \frac{r(s)}{F_{dy}(s)} = g_3 \qquad [4.6]$$

$$G_M(s) = \frac{r(s)}{M_D(s)} = g_4 \qquad [4.7]$$

4.2   Conventional car

From equation [3.74], the transfer function of the conventional car from δ_1 and δ_2 to r is:

$$\begin{aligned}
G_1(s) &= \frac{r(s)}{\delta_1(s)} = \frac{d_1}{P(s)} \\
&= \frac{C_3\mu_1 C_{\alpha 1}/mv + (s - C_1)(a\mu_1 C_{\alpha 1})/I_z}{s^2 + c_1 s + c_2} \\
&= \frac{(C_3\mu_1 C_{\alpha 1}/mv - C_1 a\mu_1 C_{\alpha 1}/I_z) + \left[(a\mu_1 C_{\alpha 1})/I_z\right]s}{s^2 + c_1 s + c_2}
\end{aligned} \qquad [4.8]$$

similarly

$$G_2(s) = \frac{r(s)}{\delta_2(s)} = \frac{d_2}{P(s)}$$

$$= \frac{C_3\mu_2 C_{\alpha2}/mv + (s - C_1)(a\mu_2 C_{\alpha2})/I_z}{s^2 + c_1 s + c_2}$$

$$= \frac{(C_3\mu_2 C_{\alpha2}/mv - C_1\, a\mu_2 C_{\alpha2}/I_z) + [(a\mu_2 C_{\alpha2})/I_z]s}{s^2 + c_1 s + c_2} \qquad [4.9]$$

Where $P(s)$ is as explained in equation [3.65]

From Ackermann et al. (2002, pg 234), it is stated when discussing comparative simulations, that for the sake of comparability, the conventional car is assumed to be a steer-by-wire vehicle equipped with the same steering actuator as the controlled car. Therefore, the transfer function from steering wheel angle to yaw rate r could be found by multiplying the transfer function as in equations [4.8] and [4.9] with the transfer function of the actuator dynamics i.e. from equation [3.74]:

$$G(s) = \frac{r(s)}{\delta_f(s)} = (G_1 + G_2)G_a$$

Where G_a is for actuator dynamics. The transfer function can be seen as follows:
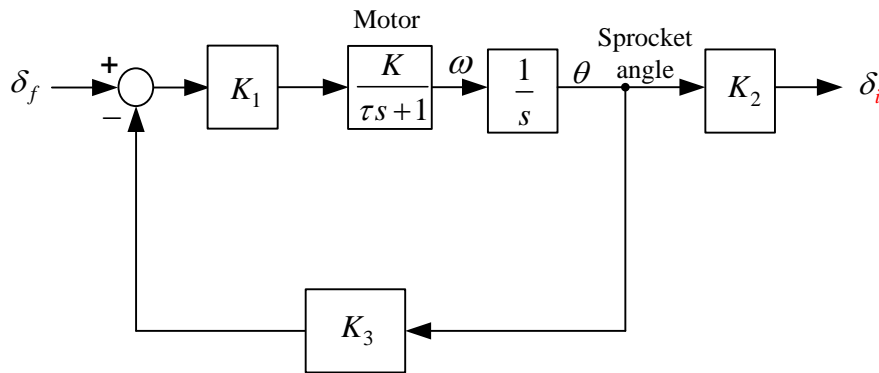
Figure 4-1:   **Actuator model**

$$G_a = \frac{K_B}{\tau s^2 + s + K_1 K_3 K} \quad \text{with}$$

$$K_B = K_1 K_2 K$$

The transfer functions for yaw disturbance input from lateral disturbance force F_{dy} and yaw disturbance moment, M_D, will be, (see equation [3.74]):

$$
\begin{aligned}
G_F(s) &= \frac{r(s)}{F_{dy}(s)} = \frac{d_5}{P(s)} \\
&= \frac{C_3/(mv) + (s - C_1)(l_{gp}/I_z)}{s^2 + c_1 s + c_2} \\
&= \frac{\left[C_3/(mv) - (C_1 l_{gp})/I_z \right] + (l_{gp}/I_z) s}{s^2 + c_1 s + c_2}
\end{aligned}
$$

[4.10]

and

$$
\begin{aligned}
G_M(s) &= \frac{r(s)}{M_D(s)} = \frac{d_6}{P(s)} \\
&= \frac{(s - C_1)/I_z}{s^2 + c_1 s + c_2} \\
&= \frac{s/I_z - C_1/I_z}{s^2 + c_1 s + c_2}
\end{aligned}
$$

[4.11]

4.3 Results

This section deals with simulated results that were done. The vehicle step responses are shown where the inputs were lateral force input and yaw disturbance torque.

4.3.1 Validation of the model

In order to check the validity of the model and the code, the system was given similar inputs and parameters to what Ackermann et al. (2002) did and the results are as shown in figure 4-2. The simulated results as seen in the graphs compare very well with what is found in the Ackermann et al. (2002), especially on page 235. The value for torque

disturbance input used was 1300Nm while the steering wheel angle step input was $0.13°$.

There is a good correlation between these two results and this stems from the fact that the two models were analysing the same physical system. Simulated results meanings are well articulated by Ackermann et al. (2002). δ_{Fcontr} and δ_{Fconv} have the same meanings as δ_1 in the nomenclature and figure 3-2, for the controlled vehicle and conventional vehicle, respectively. Here δ_s is the steering wheel angle.
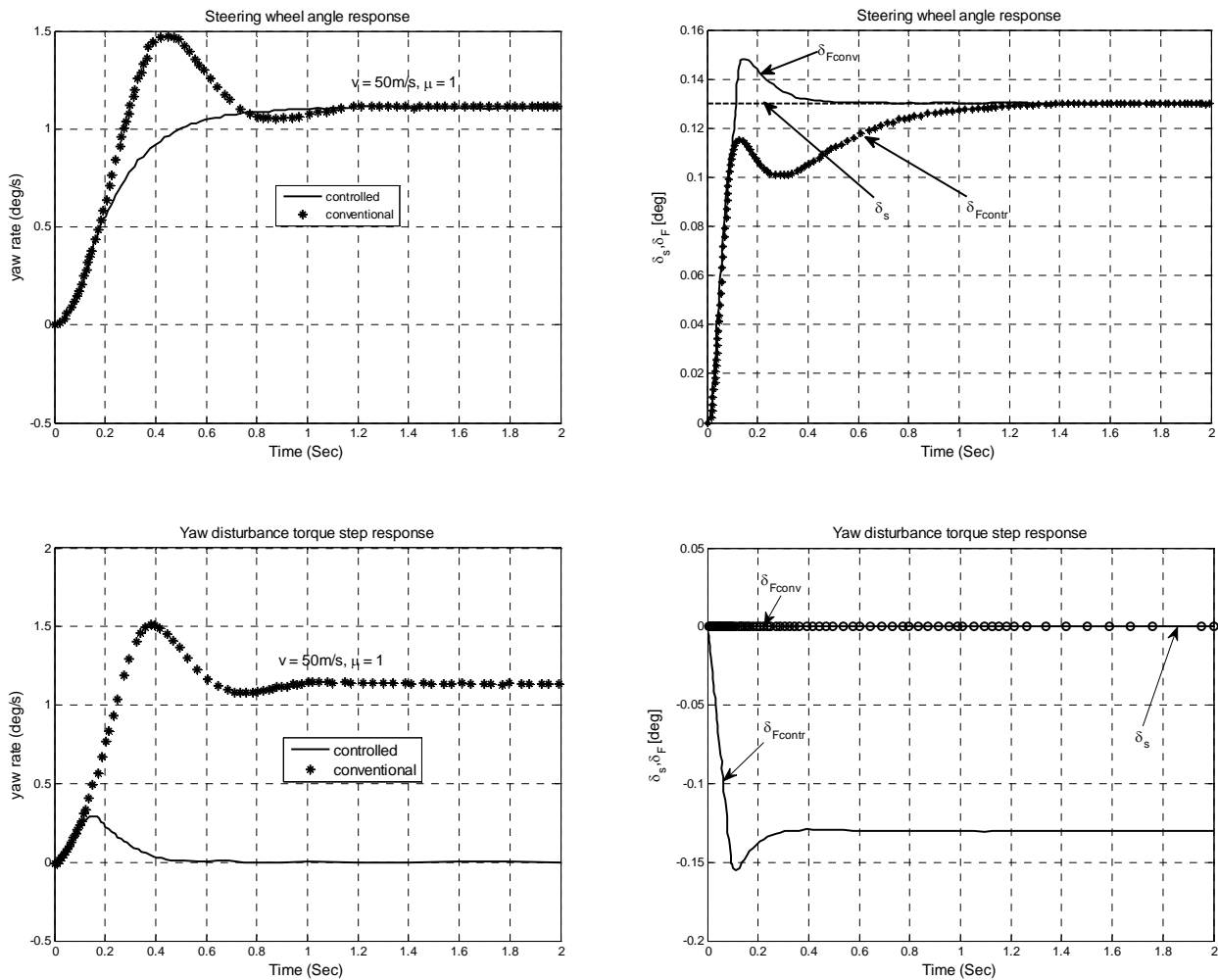
Figure 4-2:   **Simulation results at** $v = 50 \ m/s \ \mu = 1$

4.3.2   Simulations of a conventional and a decoupled vehicle

All the simulations were based on the assumption that the vehicle was travelling on a dry ground hence μ_i was taken to be equal to 1. A value of 1500N for step lateral force was always used while the disturbance yaw moment used was 1950Nm unless otherwise stated.

For the conventional vehicle with front steering only, figure 4-3, the system shows that it is oscillatory before coming to the steady state value for both the yaw torque and lateral side wind disturbance input. As for the decoupled system, the responses show that the system is able to arrest the continued rotation. The decoupled system with front wheels being steered, figure 4-4, struggles a little bit as compared to the system that combines with rear individual wheel steering, figure 4-5. Comparing graphs in figure 4-3 with graphs in figure 4-4 and figure 4-5, one can notice that the controlled system removes the effect of the disturbance, and this is evidenced by the zero steady state value, and also the reduced peak value.
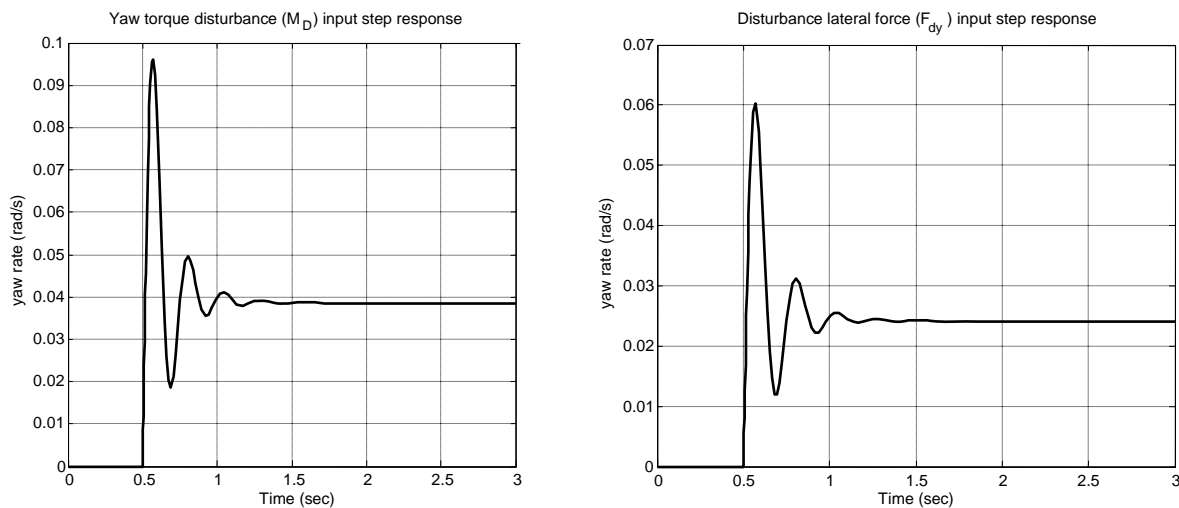
Figure 4-3:   **Step responses of conventional vehicle with front wheels steering only**

On comparing graphs 4-4 and 4-5, one will notice that graph 4-4 is oscillatory as compared to graph 4-5 and their settling time is also slightly different. Of course it can be noted that there was a price that graph 4-5 paid in that the peak is higher as compared to graph 4-4. We should keep in mind that both of them are decoupled systems only that one has both front and rear wheels steered while the other one has only the front wheels steered.
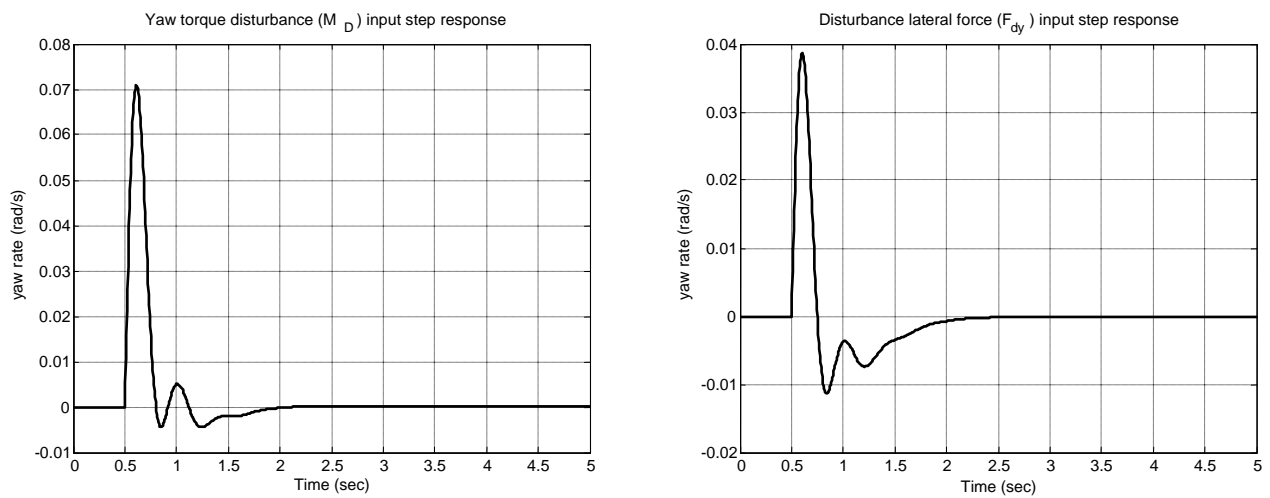
Figure 4-4:   **Step responses of robustly decoupled vehicle with front wheel steering only**
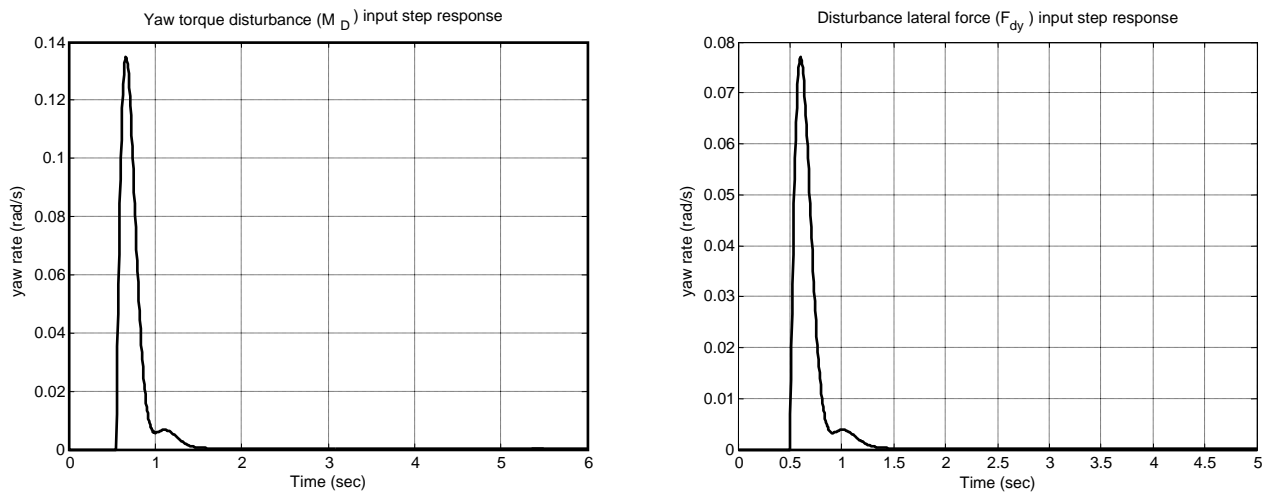
Figure 4-5:   **Step responses of robustly decoupled with front wheel steering and individual rear wheel steering**

The control laws for the rear wheels that were used in all simulations from section 4.2.1

and section 4.2.2 were $\delta_3 = \left(K_3 r_{def} \right) \left(\dfrac{s}{s+6} \right)$ and $\delta_4 = \left(K_4 r_{def} \right) \left(\dfrac{s}{s+6} \right)$ with K_3 and K_4 as

desired damping gains and r as the yaw rate and the meanings are described in section

4.2.3. δ_4 is for the rear right and δ_3 is for the rear left. The constant used were not the

same and the value used for K_3 was 9.6723×10^{-3} and the value for K_4 was

8.9593×10^{-3}. This made it easy to feed signals to left and the right wheels because of its

simplicity. This control law was chosen and used because of its simplicity. Ackerman et

al (1992, 2002) suggested and used something similar to this control law.

The rear wheel steering control angles that are proposed here cannot be accommodated

within the theory derived, but the more general equations that can be used are given in

section 4.3.3.1.

All the cases that have been presented so far under this section assume that all parameters

remain constant and that only the disturbance input to the system changes i.e. either the

input is yaw torque, M_D, or lateral force, F_{dy}. Figures 4-6 to 4-9 show the yaw rate

response of the vehicle when subjected to a lateral disturbance force under the current

control laws (unilateral decoupled vehicle response with front wheel steering only), but

with varying friction coefficients, the same friction coefficient being used at each wheel.
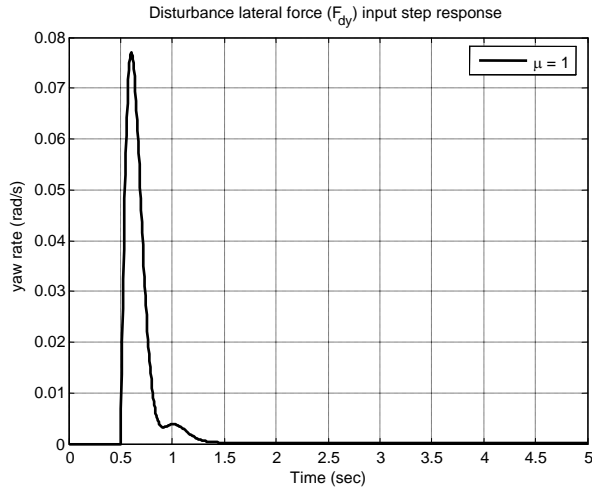
Figure 4-6: Force input response $\mu = 1$
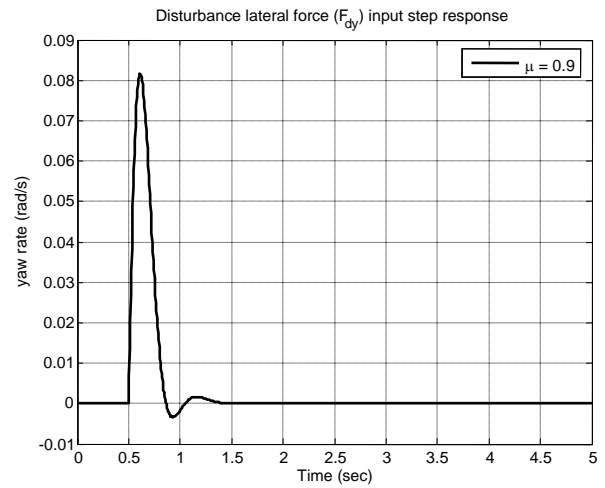
Figure 4-7: Force input response at $\mu = 0.9$
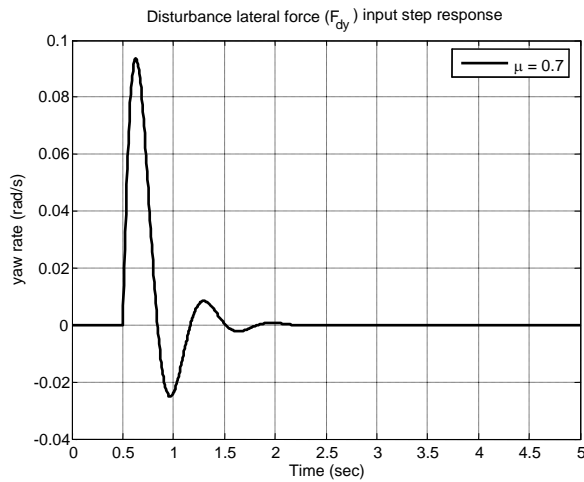
Figure 4-8: Force input response at $\mu = 0.7$
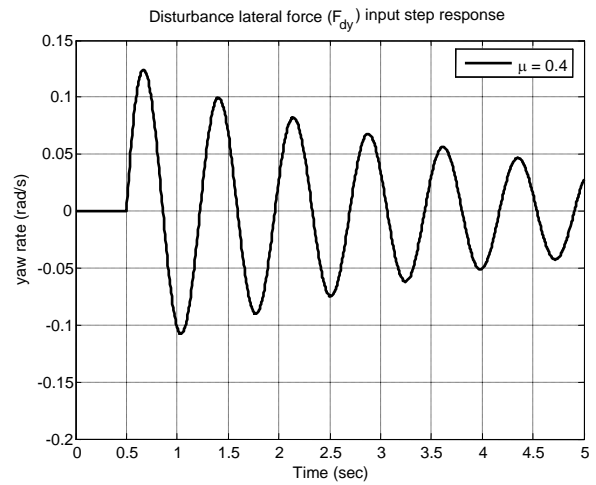
Figure 4-9: Force input response at $\mu = 0.4$

From the figures 4-6 to 4-9, it can be seen that as μ is reduced, the maximum yaw rate increases and similarly, as μ is increased, maximum yaw rate amplitude also reduces. As μ becomes smaller, the system becomes oscillatory and the converse is also true.

4.3.3 *New control laws*

There was need to come up with new control laws to enhance the concept of individual wheel steering so that one can control the wheels independently of the other. The whole

idea is to have a method of controlling the wheels that could be steered differently from each other.

4.3.3.1   Requirements for Control Law Design

According to the understanding of this author, a control law is merely a mathematical statement that helps in decision making within a control system. It not only "helps", but it also enforces (or at least tries to enforce) a certain dynamic behaviour. Consider a single steerable wheel. Let's say under certain conditions, a driver needs to generate a high lateral force from the wheel. Ordinarily he will have to increase the steering angle in order to generate the required steering force. The following were the control laws that were used in the simulations under this section.

$$\delta_{c1} = \frac{\mu_1 s}{s^2 + 5s + 10} \varphi_1(s)$$

[4.13]

$$\delta_{c2} = \frac{\mu_2 s}{s^2 + 5s + 10} \varphi_1(s)$$

[4.14]

$$\delta_3 = \left(-\frac{\mu_3 r_{def}}{k_{23} + \mu_3 k_{13}} \right) \left(\frac{s}{s+6} \right)$$

[4.15]

$$\delta_4 = \left(-\frac{\mu_4 r_{def}}{k_{24} + \mu_4 k_{14}} \right) \left(\frac{s}{s+6} \right)$$

[4.16]

with

$$\varphi_1(s) = r_{def} - \frac{l_{DP} - a}{v} sr(s)$$

[4.17]

$$r_{def} = r_{ref} - r$$

[4.18]

The chosen control laws for the rear wheels will ensure that the steering angle increases when there is an increase in the coefficient of friction and reduces the steering angle when the coefficient of friction is reduced. This is true provided that k_{23} and k_{24} are large

relative to $\mu_3 k_{13}$ and $\mu_4 k_{14}$, respectively. As for the two front steering angle control laws (equations [4.13] and [4.14]), the choice of the control laws was done to ensure that these angles return to their zero position in the steady state. These control laws are of the form of the fading integrator. According to Ackerman et al. (1992, 2002), the use of the fading integrator is to make sure that the corrective steering returns to zero in the steady state after the occurrence of the disturbance input. The whole idea is to only have this occurring for the first second after disturbance input before the driver reacts. It is further stated that this is desirable and done in order to achieve the same stationary cornering behaviour that the driver is used to and also to unload the actuator for the corrective steering. The other notable thing with the usage of fading integrators according to Ackerman et al. (2002) is that stability problems in the yaw motion are reduced. There are two types of the fading integrators used by Ackerman et al. (2002) which are second order and first linear order filters.

In view of the new control laws, equation [3.37] was reworked. Using $\delta_1 = \delta_s + \delta_{c1}$ and $\delta_2 = \delta_s + \delta_{c2}$ equation [3.37] now becomes:

$$\begin{bmatrix} \dot{\beta} \\ \dot{r} \end{bmatrix} = \begin{bmatrix} C_1 & C_2 \\ C_3 & C_4 \end{bmatrix} \begin{bmatrix} \beta \\ r \end{bmatrix} + \begin{bmatrix} \dfrac{\mu_1 C_{\alpha 1}}{mv} & \dfrac{\mu_2 C_{\alpha 2}}{mv} & \dfrac{\mu_3 C_{\alpha 3}}{mv} & \dfrac{\mu_4 C_{\alpha 4}}{mv} \\ \dfrac{a\mu_1 C_{\alpha 1}}{I_z} & \dfrac{a\mu_2 C_{\alpha 2}}{I_z} & -\dfrac{\mu_3 l_r C_{\alpha 3}}{I_z} & -\dfrac{\mu_4 l_r C_{\alpha 4}}{I_z} \end{bmatrix} \begin{bmatrix} (\delta_s + \delta_{c1}) \\ (\delta_s + \delta_{c2}) \\ \delta_3 \\ \delta_4 \end{bmatrix} + \begin{bmatrix} \dfrac{1}{mv} & 0 \\ \dfrac{l_{gp}}{I_z} & \dfrac{1}{I_z} \end{bmatrix} \begin{bmatrix} F_{d_y} \\ M_D \end{bmatrix}$$

$$\begin{bmatrix} \dot{\beta} \\ \dot{r} \end{bmatrix} = \begin{bmatrix} C_1 & C_2 \\ C_3 & C_4 \end{bmatrix} \begin{bmatrix} \beta \\ r \end{bmatrix} + \begin{bmatrix} \dfrac{\mu_1 C_{\alpha 1}}{mv} & \dfrac{\mu_2 C_{\alpha 2}}{mv} & \dfrac{\mu_3 C_{\alpha 3}}{mv} & \dfrac{\mu_4 C_{\alpha 4}}{mv} \\ \dfrac{a\mu_1 C_{\alpha 1}}{I_z} & \dfrac{a\mu_2 C_{\alpha 2}}{I_z} & -\dfrac{\mu_3 l_r C_{\alpha 3}}{I_z} & -\dfrac{\mu_4 l_r C_{\alpha 4}}{I_z} \end{bmatrix} \begin{bmatrix} \delta_{c1} \\ \delta_{c2} \\ \delta_3 \\ \delta_4 \end{bmatrix} + \begin{bmatrix} x_1 & \dfrac{1}{mv} & 0 \\ x_2 & \dfrac{l_{gp}}{I_z} & \dfrac{1}{I_z} \end{bmatrix} \begin{bmatrix} \delta_s \\ F_{d_y} \\ M_D \end{bmatrix}$$

Where:

$$x_1 = \frac{\mu_1 C_{\alpha 1} + \mu_2 C_{\alpha 2}}{mv}$$

$$x_2 = \frac{a\left(\mu_1 C_{\alpha 1} + \mu_2 C_{\alpha 2}\right)}{I_z}$$

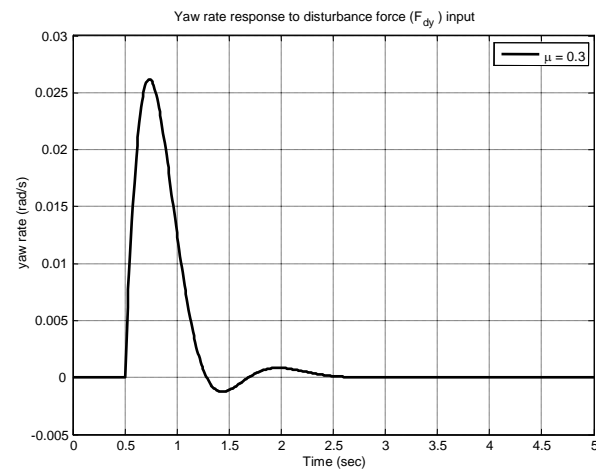In all the simulation cases, the value used for step disturbance side (cross) wind force is

1500N and the fading integrator used is $\dfrac{s}{s^2 + 5s + 10}$.

4.3.4 Simulations of different coefficient of friction μ

Figures 4-10 and 4-11 are vehicle responses when the all the four wheels have the same

coefficient of friction μ. All the wheels are assumed to be under the same road

conditions.
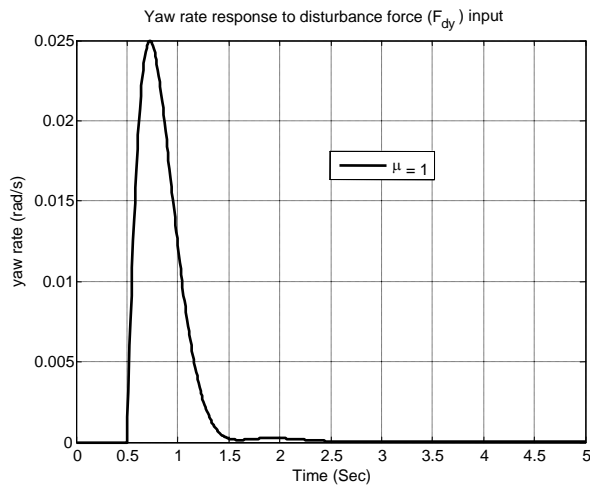
4-10   Force input response $\mu = 1$ **4-11   Force input response at $\mu = 0.3$**

Comparing figures 4-10 and 4-11 to figures 4-6 to 4-9, it can be seen that the oscillations

have reduced when considering lower coefficients of friction.

The results given in figure 4-12 show rear wheels steer angle responses. The simulations

that were done in this case are where the left hand side of the vehicle is on the different

road conditions compared the right hand side. For example, the left hand side wheels could be in mud while the right hand side wheels could be on dry tar mark road. We are going to monitor what will be happening to the rear wheels (δ_3 and δ_4). The coefficient of friction for the left wheels, corresponding to δ_1 and δ_3, will be the same and μ will be varied; at the same time, the coefficient of friction for the right hand side wheels, corresponding to δ_2 and δ_4, will be the same and it will remain constant at 1.
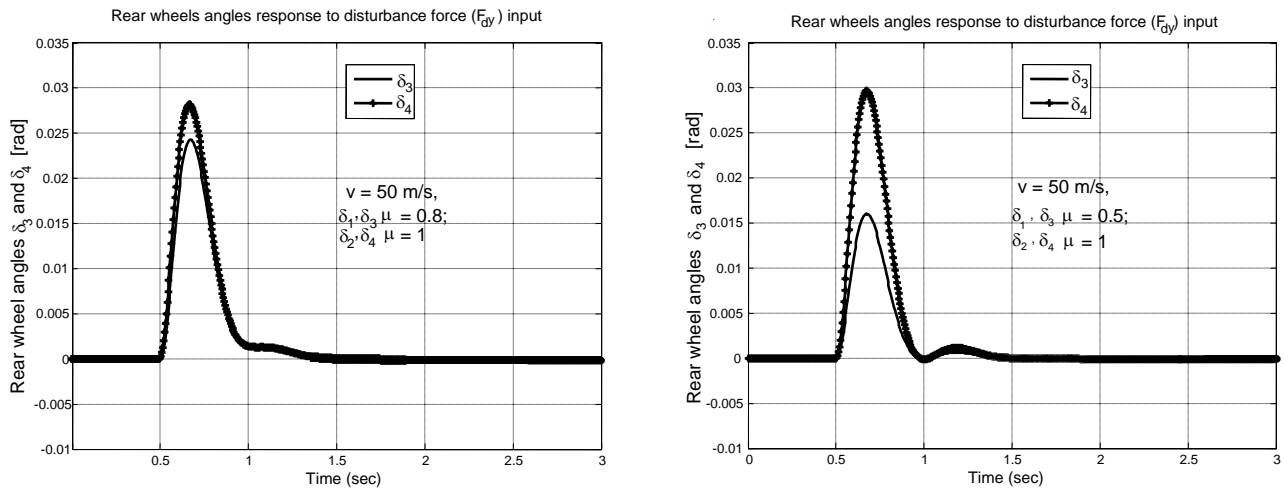
Figure 4-12: Vehicle disturbances response to different μ

The results as seen in figure 4-12 show that when two sides are on different road conditions, the model is able to turn more on the hard side (larger μ) and it is also able to turn less on the side with lower value of coefficient of friction. This shows that it is possible to control each individual wheel independently.

5   IMPLEMENTATION OF INDIVIDUAL WHEEL STEERING

5.1   *Introduction*

Theoretical modelling and analysis of an individual wheel steering (IWS) system was done when all information was gathered both from available literature as well as from the existing 4WS experimental vehicle that is in the SASOL Lab. This vehicle, figure 5-1, used to have the normal mechanical front wheel steering while the rear wheels were controlled through steer by wire. The whole 4WS was reworked in order to achieve individual wheel angle steering. Electric actuators were installed for both front and rear, on each wheel, to replace the previous steering system that included electrically actuated hydraulic power steering on the two rear wheels only.

The rear wheel steering rack with power steering was disabled. Both the front and the rear tie-rods were replaced by linear actuators. These were designed and built specifically for this project and the purpose of these linear actuators were to effect the individual wheel steering control. The normal front wheel steering via the rack and pinion system was still partly available for the driver to control the front wheel steer angles.

Figure 5-1:   **Experimental vehicle**

5.2   *Motor characterisation*

A Bosch wiper motor, including its reduction worm gear box, as used in a BMW 325i model, as shown in figure 5-2, was used in each of the linear actuators. Furthermore, it is worth mentioning that one can use either of two methods to control a DC wiper motor: an armature control or pulse width modulation (PWM). Inside the position feedback control loop, in the forward path, the DC motor and its control works as a speed control sub-system, regardless of whether one uses armature control or PWM. The DC motor in speed control can mathematically be modelled as an armature controlled DC motor and can be represented as a first order equation as shown in equation [5.1], after

approximating $L_a << R_a$, as given by Dorf et al. (2001), equation [2.69], where K and τ can be determined experimentally.

$$\frac{\omega(s)}{V_a(s)} = \frac{K}{\tau s + 1} \qquad\qquad [5.1]$$
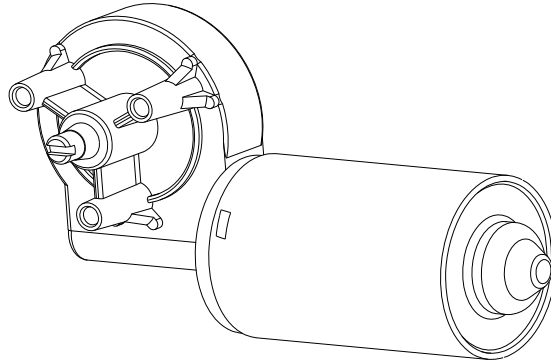
Figure 5-2:   **Wiper motor sketch**

Because of lack of information about this wiper motor, several tests were conducted to determine its characteristics, primarily the gain K and time constant τ as shown in equation [5.1]. Figure 5.3 shows the setup for the determination of the motor characteristics. A tacho-generator was connected to the shaft of the motor, to generate a voltage output signal proportional to the motor speed. The output from the tacho-generator and the input from the motor were measured using a digital oscilloscope. The data were extracted from the oscilloscope using a computer. Tacho-generator was used only for the purpose of the characterization exercise. It does not form part of the actual actuator control system.
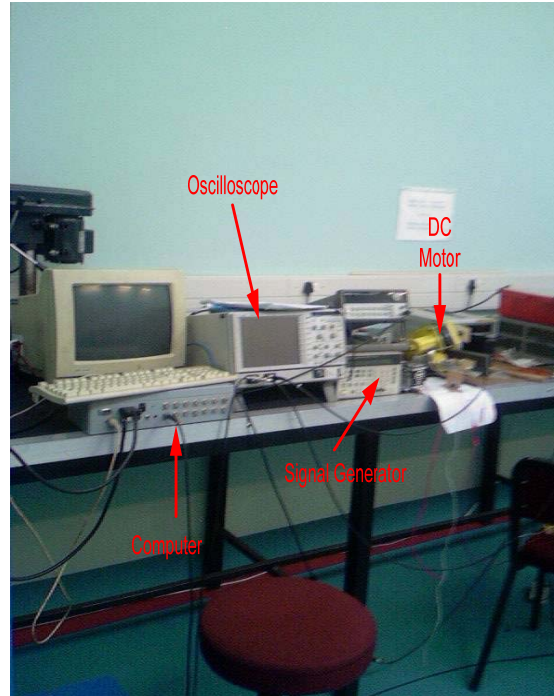
Figure 5-3: **Motor tests setup**

Figure 5-4 shows the response of the motor to step input. The first experiments done were to determine motor time constant τ. This was done in order to find out if the wiper motor to be used meets the desired requirements.
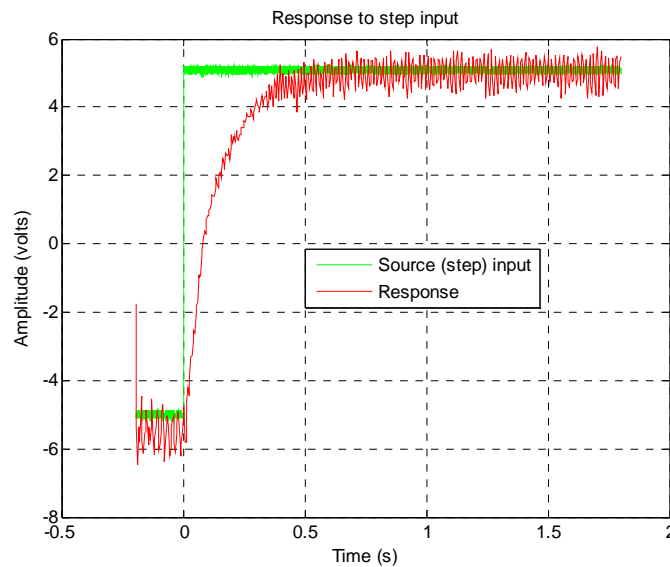
Figure 5-4: **Motor response to a step input**

55

Figures 5-4 shows motor response to a step input and amplitude is in volts. The response graph has been multiplied by the reciprocal of the DC gain, which is why in the steady state the two graphs fall on top of one another. From this figure, it can be noted that the motor attained its steady state in less that 1 sec. This exercise was done to make sure that motors used fell within the specifications one of which was to be able to attain its steady state in less than 1 sec. This was open loop input – output relationship. To find the settling time of the system, locate the time on the plot when the magnitude crosses the desired percentage of the final value. For instance to find the 10% settling time of this system, look for where the response reaches 90% of the final value. The time constant, τ, of the system is the time at which the response is $\left(1 - 1/e\right)$ times by the final value. The relationship between the time constant and the pole of a system is: pole = -1 / τ. Other handy approximate relations for finding the time constant are:

τ = 10% Settling Time / 2.3 or

τ = 5% Settling Time / 3 or

τ = 2% Settling Time / 4.

From the graphs, the average τ was found to be equal to 0.1339 sec. This was deemed acceptable.

The next step was to find the DC gain, K, of the motor. The DC gain is the ratio of the steady state step response to the magnitude of a step input. The steady state step response can be determined from the plot of the step response like one shown in figure 5-4. The value of gain K was found after taking into consideration the calibration value of the

tacho-generator as well as the gain from gear ratio of the wiper motor gear box. The average value of DC gain that was found was 9.972 $rad / s / v$.

5.3   *Potentiometer characterisation*

For the linear actuator to work properly there was need to create a position control system, with position feedback of some sort. After considering all the possibilities, it was decided to measure the angle of rotation of the output shaft of the wipe motor gearbox for the purposes of position feedback. A multi-turn potentiometer was used for that purpose as an angular position feedback transducer. Figure 5-5 shows the assembly used in finding the characteristics of the multi-turn potentiometer that was used as an angle feedback sensor. The body of the Potentiometer is fixed to the wiper motor chassis to prevent it from moving. The shaft of the potentiometer was inserted into a cork coupling that was fixed to the base as shown. When the motor is turning, it rotates the shaft of the Potentiometer. As the shaft turns, the voltage output can be measured and converted to the angle that the sprocket has turned.
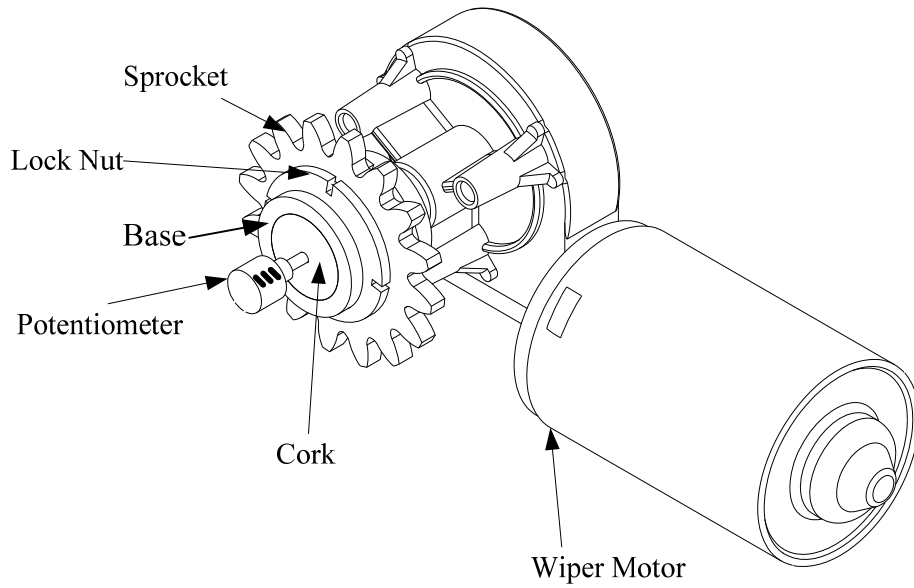
Figure 5-5:　　　**Potentiometer connection sketch**

The unit shown on figure 5-6 shows the actuator as assembled to the vehicle.
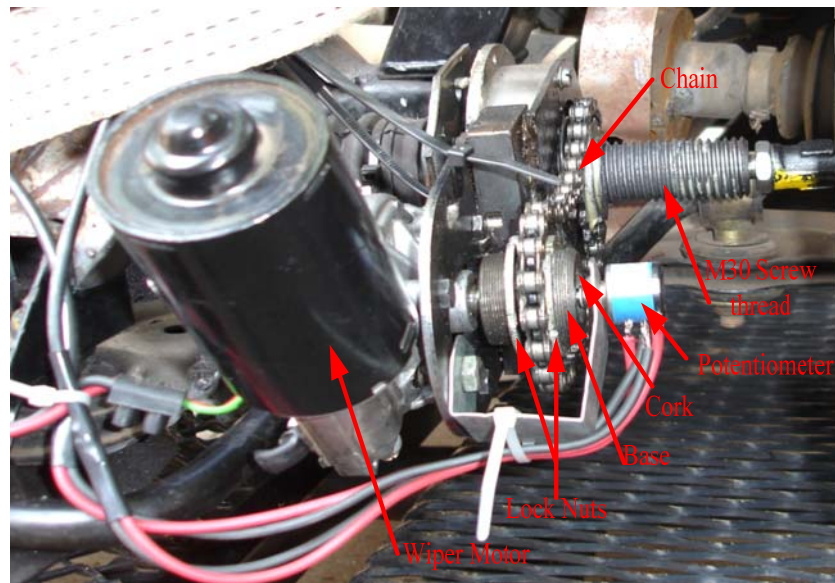

Figure 5-6:　　　**Actuator unit**

Experiments were done and the relationships below were found by measuring potentiometer angle, wheel angle and voltage output from the potentiometer. The calibration of the potentiometer was done by using the dividing head and indexing plate in the machine shop. The base of the potentiometer was clamped while turning the indexing plate. The potentiometer had 10 complete turns. Voltage measurements were taken for every complete turn of the knob of the potentiometer. The results were plotted for voltages against potentiometer angle.

The next stage was to measure the wheel angle and then measure the potentiometer voltage. This was done to find the relationship between the potentiometer voltage and the wheel angle. The first step was to zero all the wheels by aligning them. When the wheels are aligned, then that is the zero point for the potentiometer. A hard paper was stuck to the ground and then a straight edge was used to mark a straight line on the paper as the zero angle. The wheel was then turned using the actuator. The turning was not done continuously; it was done by starting and stopping the actuator. Every time when the actuator was stopped, successive lines were drawn using a straight edge on the paper that was stuck to the ground. Voltage measurements from the potentiometer were taken at every stop. This was done in both directions of the wheel turning and the same procedure was repeated on all the four potentiometers and all the four wheels. Angles were read off from the paper later on. The measured potentiometer voltage values for the wheels angle were plotted.

A mathematical relationship stemming from linear progression between the turn of the potentiometer knob for voltage and wheel angle was developed, and this was included in

the main algorithm. By using Matlab, the equation that came out was $y = 0.28x + 0.017$

where y is the wheel angle and x is the potentiometer voltage.

The graphs in figures 5-7 and 5-8 show the relationship between potentiometer voltage and Potentiometer angle as well as the relationship between potentiometer voltage and wheel angle.
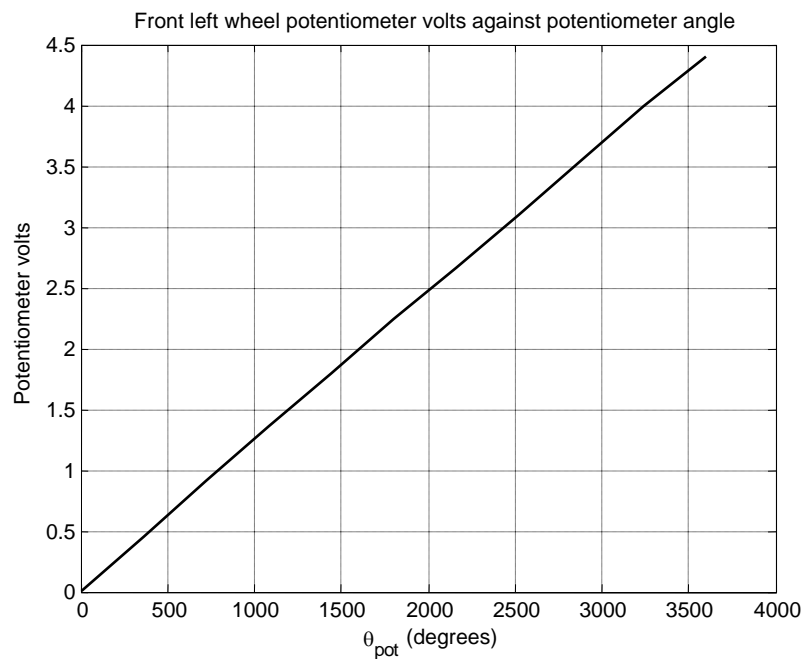

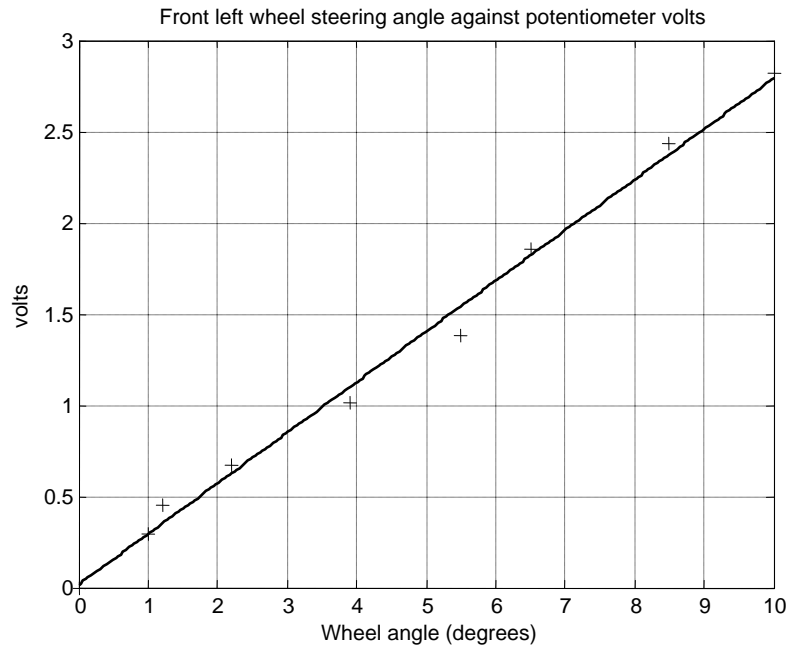**Figure 5-7:**   **Graph of potentiometer angle against potentiometer volts**

Figure 5-8:   Graph of wheel angle against Potentiometer volts

5.4   *DC motor controller*

The circuit in figures 5-10 and 5-11 were built to provide an interface between the computer and the motor. Power is supplied from the car battery through point *a* (in the red circle). The signal that controls the speed of the motor enters through point *b*. Part A (in green) generates the pulses for the PWM and passes these to the LMD18200 chip, which drives and controls the speed of the motor. The PWM was used for the DC motor speed control sub-system. The circuit to generate pulses uses two 555 ICs connected as shown. A 7805 regulator is included to restrict voltage to and from part A to 5 volts because the computer voltage signals can only go to the maximum of 5 volts. Pulses from part A enters part B (in green) through point *d*. The decision from the computer to change direction enters the chip at pin number 3 through point *c*. This tells the chip to turn the motor either clockwise or anticlockwise.
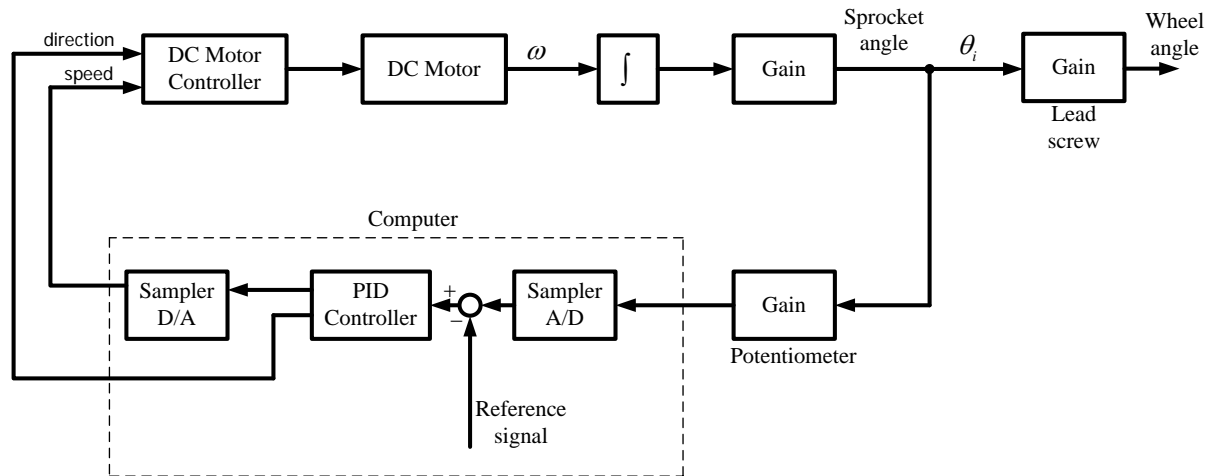
Figure 5-9:   **Actuator block diagram.**

Figure 5-9 shows a single actuator block diagram. All that is inside the dashed line was implemented in the computer and a single computer was used for all four actuators and also to run the control algorithm, which determined the input/reference signal to all four actuators. The gain after the integrator is the gear ratio of the worm gear. Downstream of the point where the sprocket feedback angle is picked, there is a gain block containing the pitch of the lead screw that translates the sprocket rotation angle into a rectilinear displacement, (the chain drive had a gain of 1).
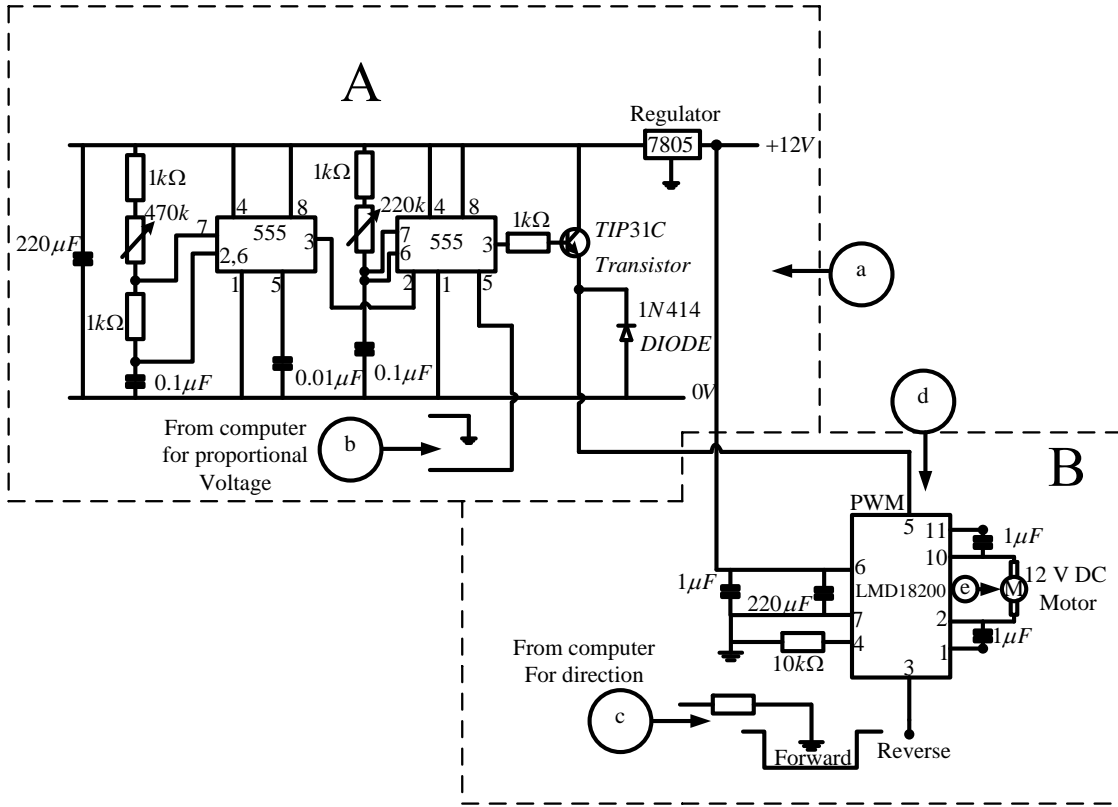
Figure 5-10:   **DC Motor Controller circuit diagram**
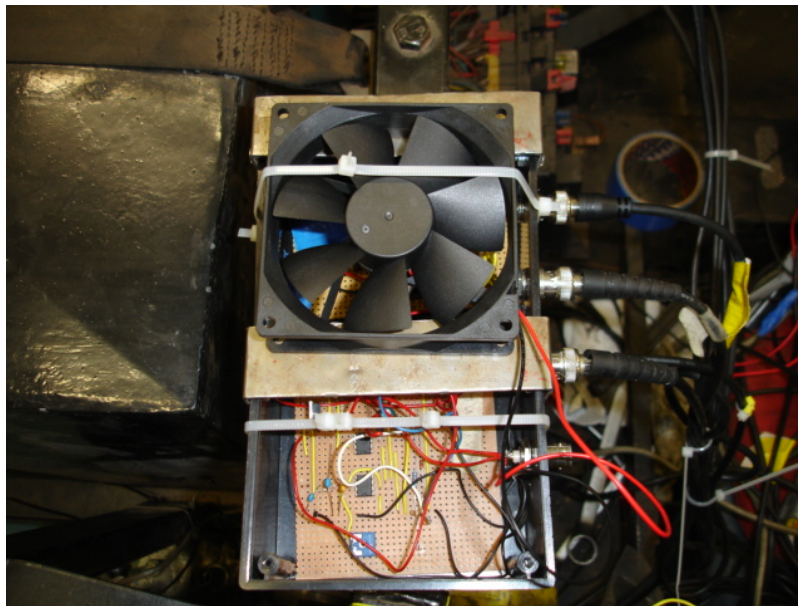

Figure 5-11:   **DC motor Controller circuit box**

A cooling fan was used to cool down the LMD18200 chip, which otherwise overheats and then shuts itself down
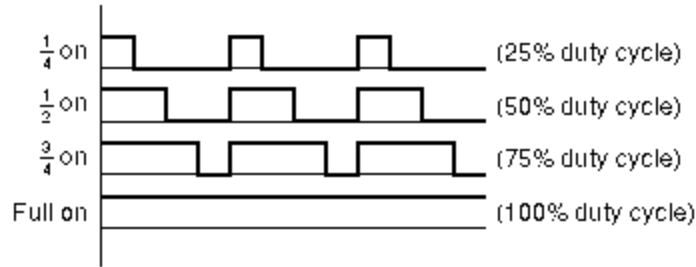

Figure 5-12:   Illustrating the principle of Pulse Width Modulation, National Semiconductors

(2005)

Figure 5-12 shows the concept of PWM. If the motor is to turn at full speed, the system has to supply 100% duty cycle pulses. In order to reduce the speed of the motor, there should be a supply of pulses as shown in figure 5-12 depending on the desired speed.
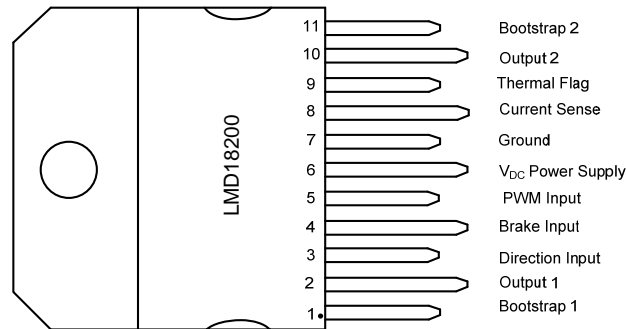

Figure 5-13:   LMD18200 chip, National Semiconductors (2005)

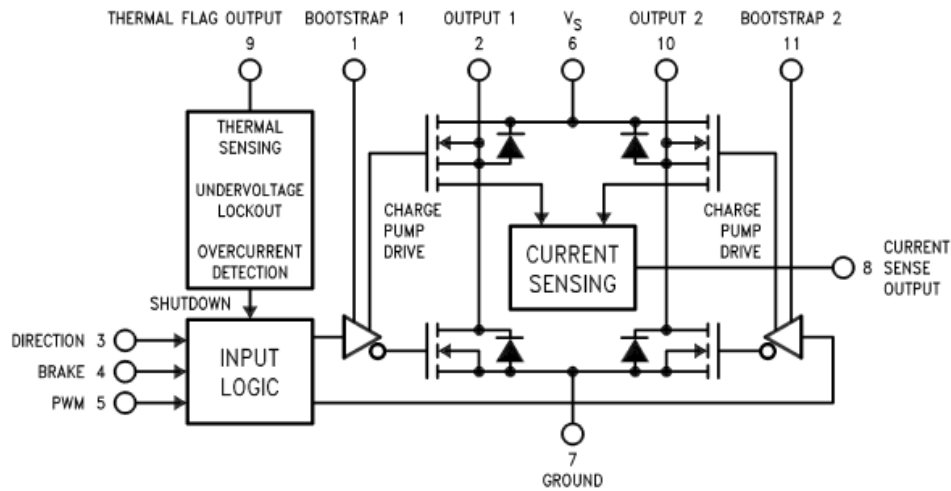Figure 5-13 shows an LMD18200 chip which works as an H-Bridge as illustrated in figure 5-14.

Figure 5-14:   **LMD18200 circuit diagram, National Semiconductors (2005)**

5.5   *Actuator assembly*

The whole actuator comprised the DC motor controller as well as the actuator assembly as shown in figure 5.15 (see also figure 5-6). The actuator assembly consisted of the Bosch DC motor, a chain, an internal threaded hub and housing, a lead screw, and a bearing as the major components, as shown in the exploded view sketch of figure 5-16. On the inboard side, the actuator was connected to the chassis, in the case of the rear actuators, or the steering rack, in the case of the front actuators, via a universal joint, while the outboard end was connected to the hub assembly via a spherical joint, similarly to a normal tie rod end connection. The inboard universal joint was used, rather than a spherical joint, to support the actuator against possible rotation about its axis, for example due to the offset weight and reaction torque of the DC motor. The lead screw and the internal threaded hub were arranged in such a way that the lead screw could move in and out of the actuator assembly as the motor is rotating. As can been seen from figure 5-16, the actuator is not sealed. This was due to space limitations, and because of the preliminary and experimental nature of the setup.

Figure 5-15:   Actuator – hub assembly connection

Figure 5-15 shows one actuator, connected to the right rear wheel, replacing the right rear tie rod of the original four wheel steering system.
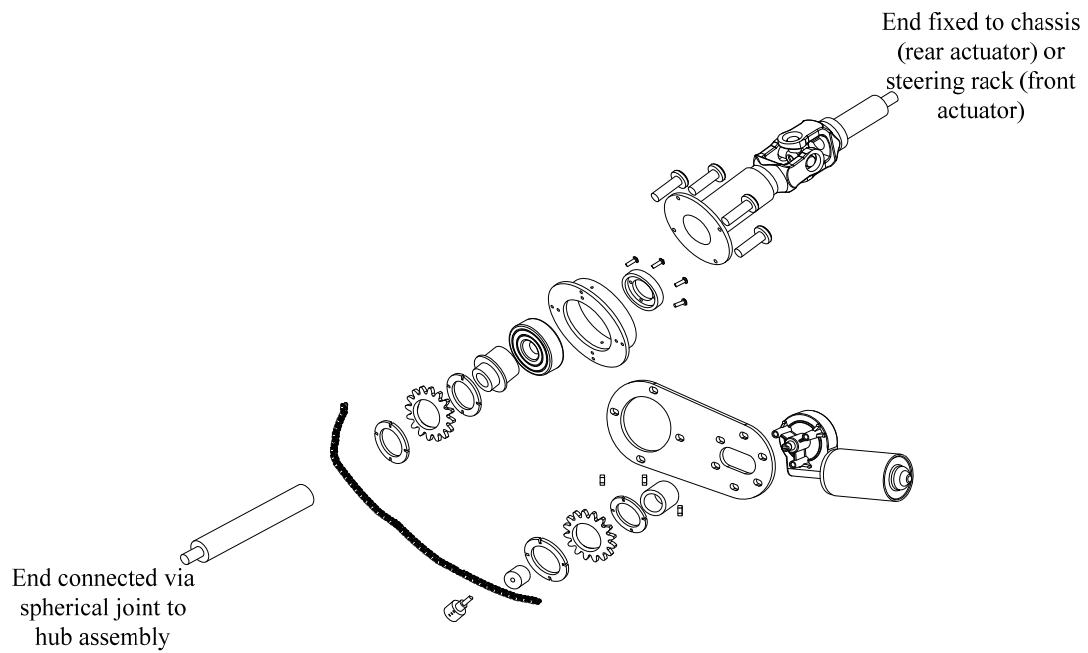
End fixed to chassis
(rear actuator) or
steering rack (front
actuator)

End connected via
spherical joint to
hub assembly

Figure 5-16:   **Actuator exploded view**

6   EXPERIMENTAL SETUP

This chapter describes the experimental setup, experimental tests that were carried out and the results that were obtained. Experimental tests were done for the individual wheel steering system. These tests were before expanding the mathematical model and therefore the tests did not implement the new control laws that are described in equations [4.13] to [4.18]. In other words, control laws equations [4.13] to [4.18] were never tested experimentally. More also, the experimental setup, as depicted in figure 6-1, used control law equation [3.50] for the front wheels and the rear wheel control laws mentioned on page 47, below figure 4-9.
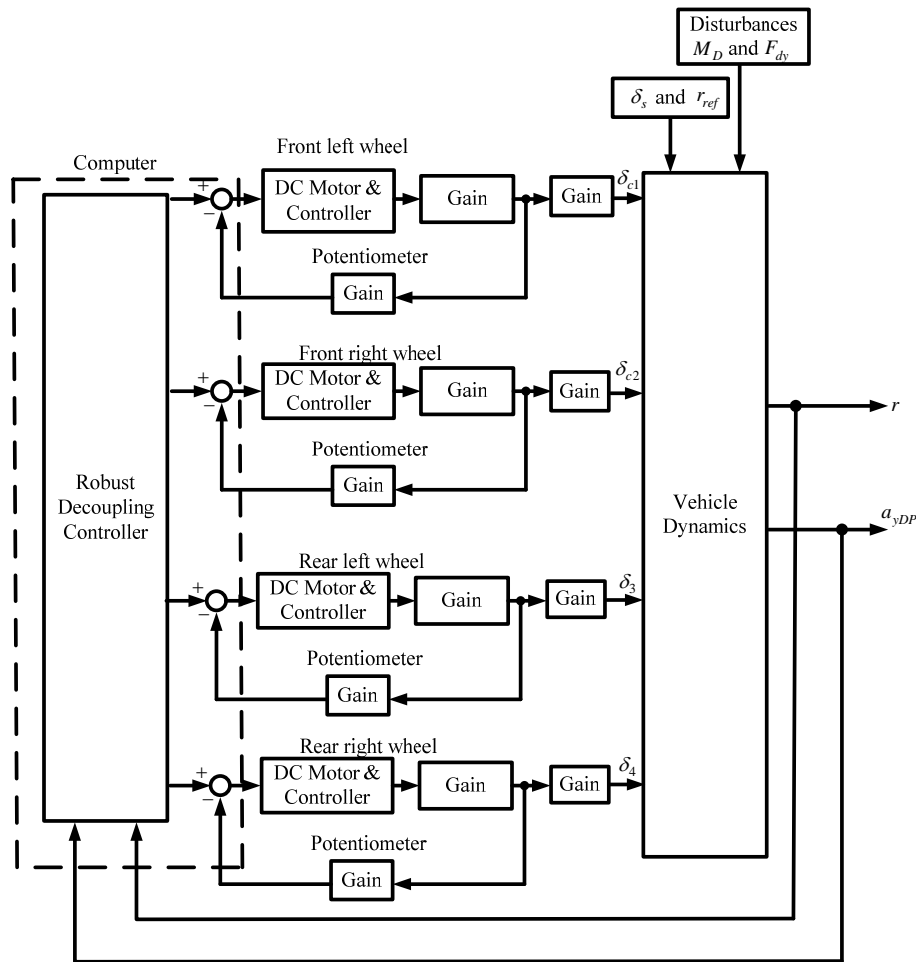

Figure 6-1:   **A sketch of experimental setup**

Figure 6-1 shows the experimental setup diagrammatically. Each wheel was controlled individually via the computer. The feedback signal from lateral acceleration shown was not used for any purpose although it is one of the outputs as shown in equation [3.70]. A yaw rate sensor was connected on the vehicle to measure the yaw rate for feedback purposes but also to have a measurable result.
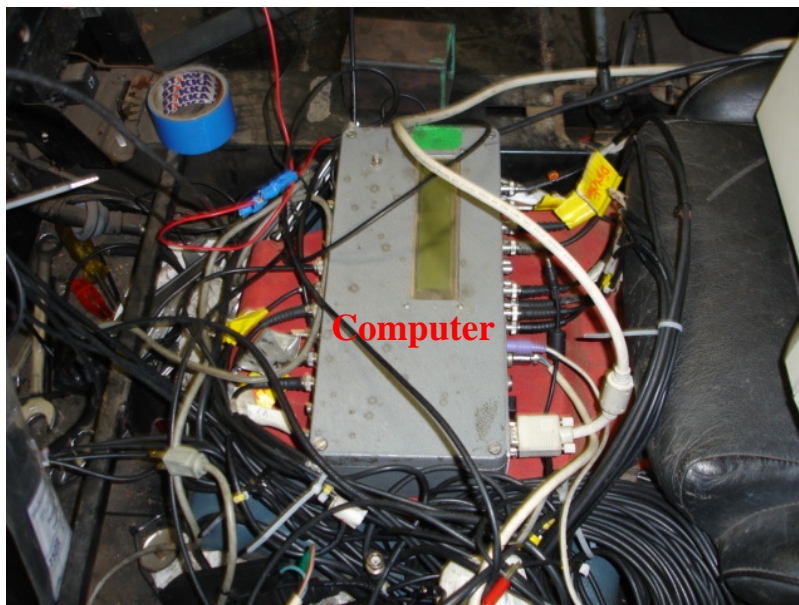

Figure 6-2:   Computer

Figure 6-2 shows a computer that was used for experiments. The output of this computer can be both analogue and digital, because it was equipped with an analogue to digital card. In this experiment, one analogue and one digital output was used for each steering actuator. The analogue output was used for control voltage while the digital output was used to switch direction of the dc motor in the actuator. The output voltage from the computer was used to change the speed of the motor. If the digital output was 0 the motor turned in one direction and if the output was 1 the motor turned in the opposite direction.

6.1   *Experimental Results*

There were two sets of experiments that were conducted to validate the proposed theories as will be discussed in section 6.1.1 and section 6.1.2. The driver kept the steering wheel straight in most of the tests that were done. The exceptions were on a number of tests where the driver had to induce sinusoidal input from the steering wheel. This was to ensure that there is separation of the driver task and that of control system. The driver's job had to do with path tracking while the control system had to control the yaw rate.

6.1.1   No input from the steering wheel

It was decided to employ uneven braking between the left and right wheels to induce a disturbance moment on the vehicle during road tests. For this purpose the brake calliper of the left front wheel was taken off the disk, thus disabling braking on that wheel. The driver then had to brake hard to induce a disturbing moment. The advantage of using this method to generate a yaw moment is that it is cheap. On the other hand, it is unlikely that this scenario will be encountered in a real life situation. It was done purely for experimental purposes. Instead, it would have been better to use wind generators to create side wind disturbance, but such generators were not available. The results provided in figures 6-3 to 6-9 are from the test run that was seen to be successful. The only known parameter is the speed since the successful test was done at a speed of 50 km/h at the time of braking. It was difficult to measure other parameters like the generated yaw torque from braking. The other tests were partially successful while other tests were not very successful as will be highlighted later.
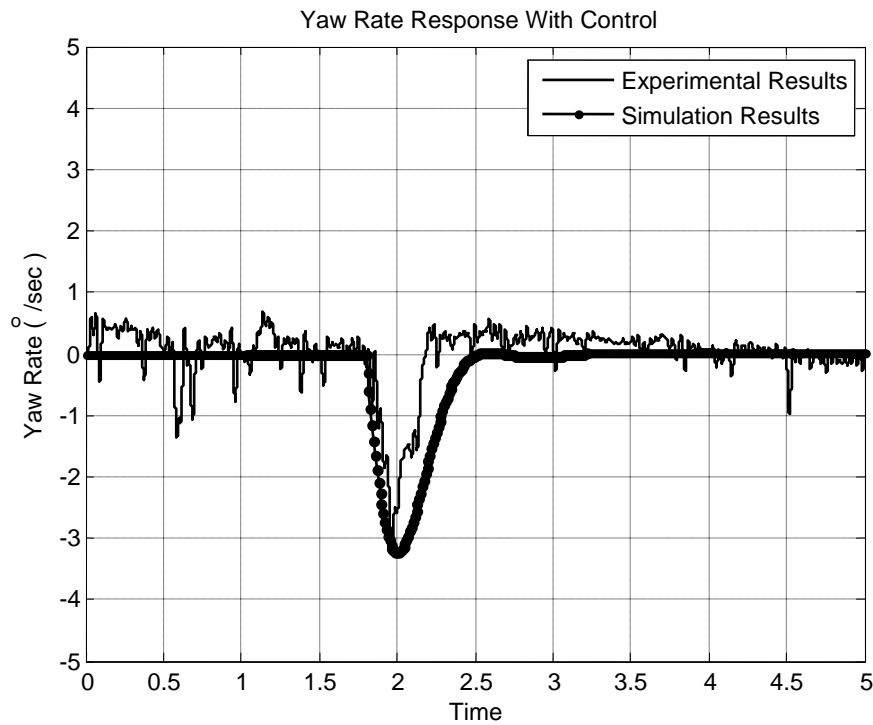
Figure 6-3:   **Controlled vehicle yaw rate response.**

Figure 6-3 shows the comparison between simulated and experimental results. The brakes were applied when the vehicle was travelling at a speed of 50 km/h. Because of lack of other information, and lack of measuring methods, some of the parameters were assumed for simulation purposes. For example, to know how much brake force and the size of yaw moment created during the period that the brakes were applied, were difficult.

Figures 6-4 to 6-7 show the comparison between the experimental and the simulated results of each wheel.
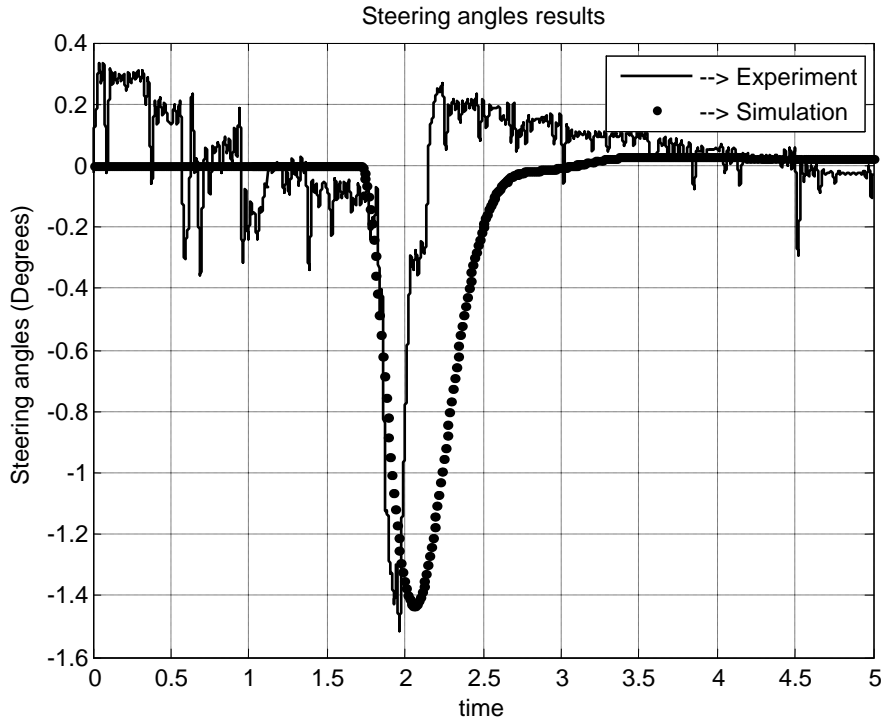
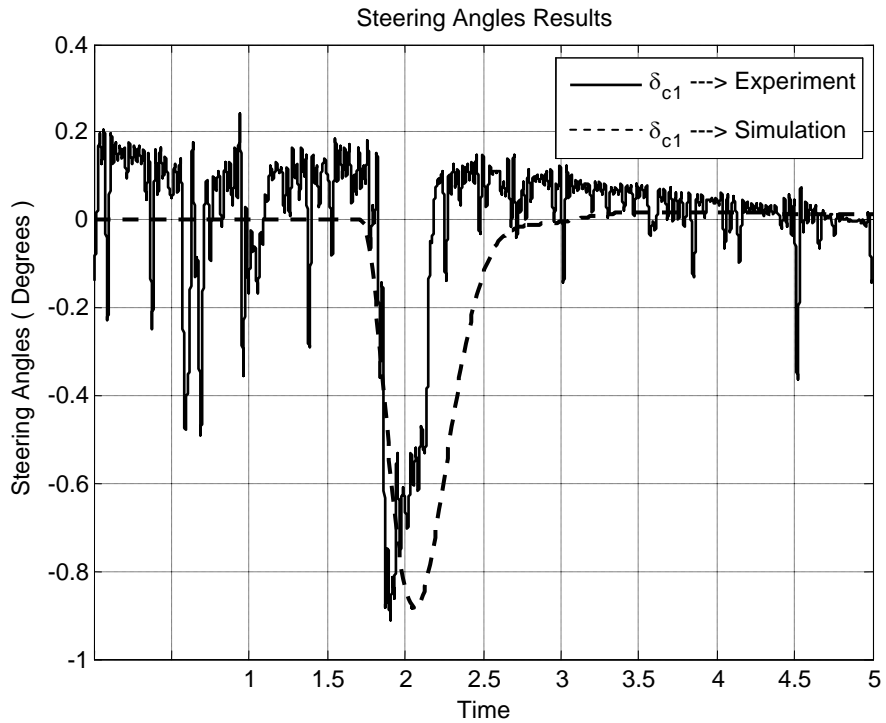**Figure 6-4:**   **Front right additional steering angle response**

Figure 6-5:   **Front left additional steering angle response**
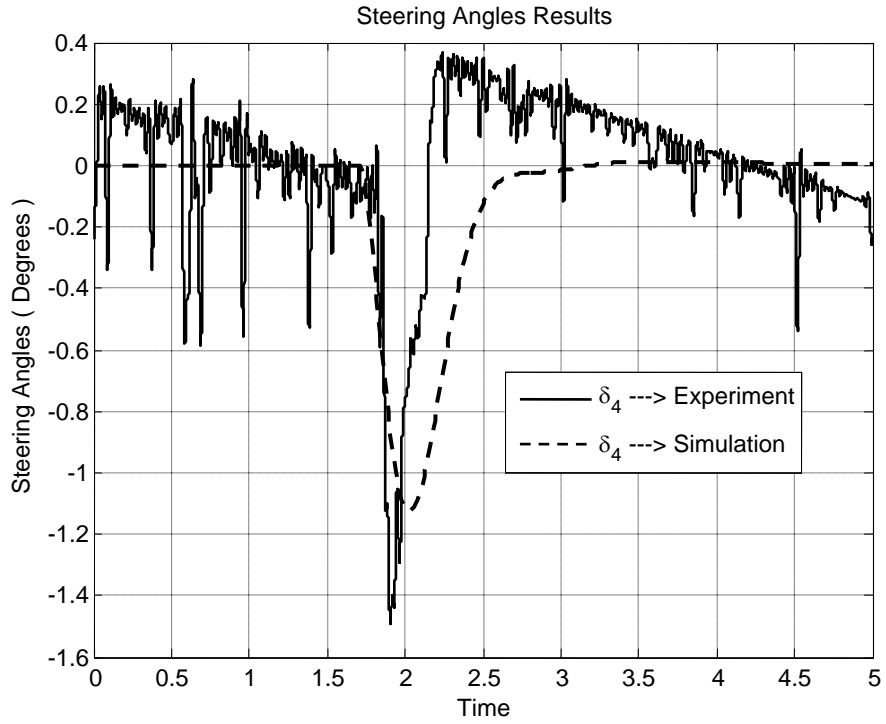
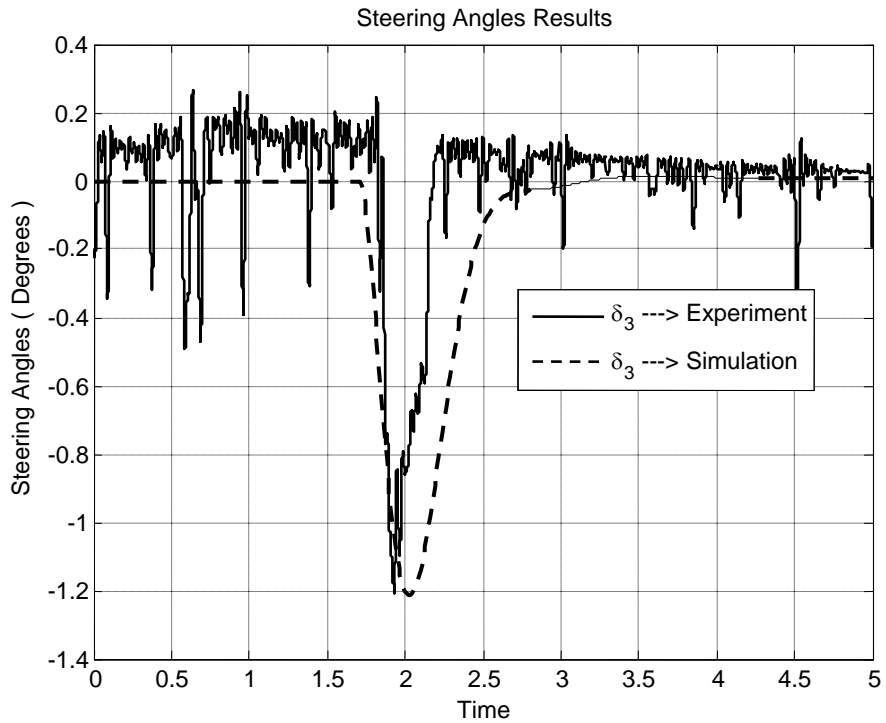**Figure 6-6:   Rear right steering angle response**

Figure 6-7:   Rear left steering angle response

73

6.1.2   Sinusoidal input from the steering wheel

Figures 6-8 and 6-9 show the yaw rate response of the test vehicle to sinusoidal input that was done through the steering wheel with the control system either inoperative (figure 6-8) or operative (figure 6.9)   and the vehicle travelling at 50 km/h. The reason why a sinusoidal input test was done was because it was thought that the controlled system could be fooled to think that the yaw that resulted from the driver giving a sinusoidal steering input was actually some disturbance that it should reject. Hence we expected that a successful test would be indicated by a reduced amplitude in the sinusoidal yaw rate variation, in the case of the controlled car. That the yaw rate would reduce to zero after the test is not an indication of success, because any stable motorcar will have a zero yaw rate in the steady state after a sinusoidal steering input was removed. From figure 6-9, it can be seen that the controlled car has a smaller variation in yaw rate than the uncontrolled car, figure 6-8. The test driver tried to use the same magnitude of sinusoidal excitation in the two cases, even though this is a subjective measure.
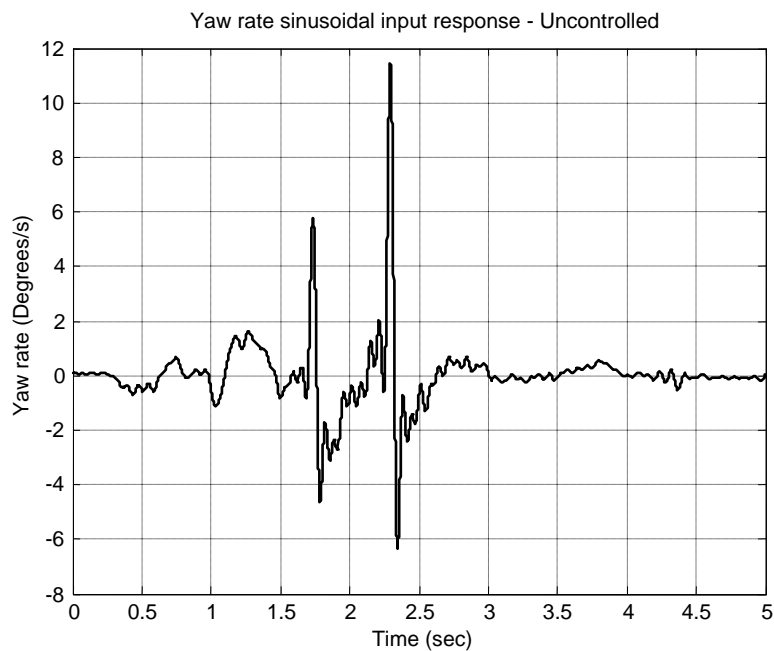
Yaw rate sinusoidal input response - Uncontrolled

Figure 6-8: **Uncontrolled vehicle test result at 50 km/h**

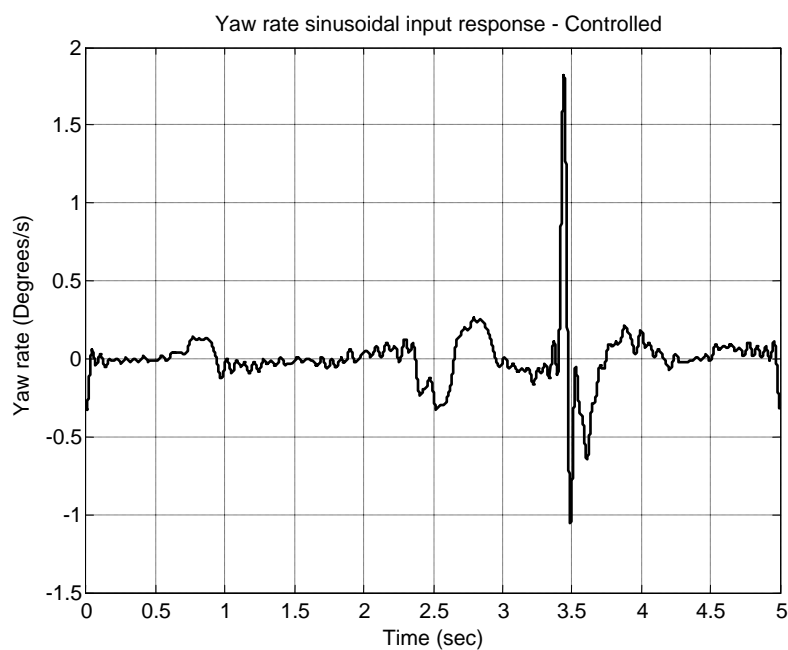Yaw rate sinusoidal input response - Controlled

Figure 6-9: **Controlled vehicle test result at 50 km/h**

There were other tests that were done at lower speeds, the results of which showed that the rear wheels did not respond satisfactorily, as shown in the figure 6-10. It was observed that at lower speeds, the rear wheels failed to respond presumably because of weight. The engine of the vehicle is mounted at the rear and as a result it was hard for the wiper motors at the back to steer the rear wheels at the lower speeds. It can be noted that the response from the front wheels is very small. This may also mean that the command signal to the two rear actuators was within the dead band of the rear actuators. The higher vertical wheel loading on the rear wheels due to the engine weight would have caused a larger dead band in the case of the rear wheels, compared to the front.
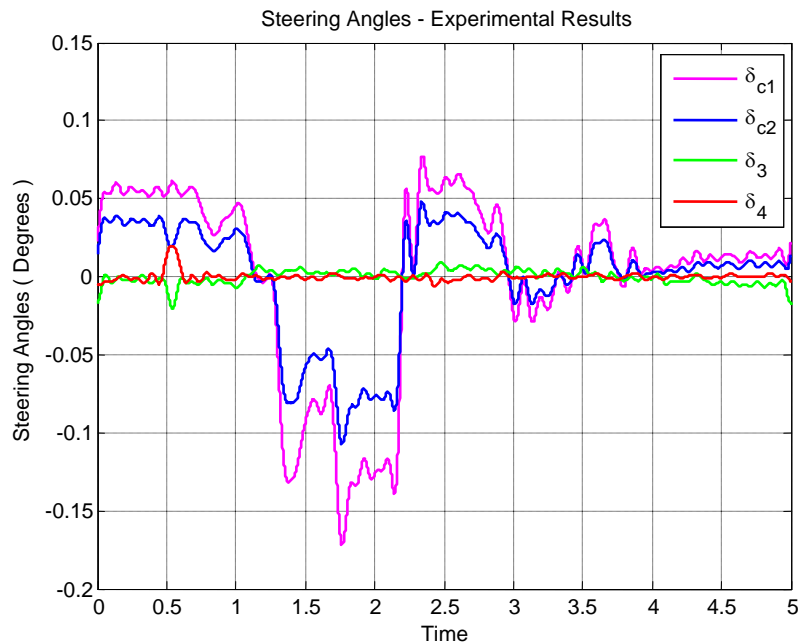

Figure 6-10:   **Steering angles response at low speed (20 km/h)**

Figure 6-10 shows a test result that was conducted at an approximate sinusoidal disturbance input through the steering wheel while the vehicle was travelling at a speed of 20 km/h. The δ_3 and δ_4 curves are not responding the same perhaps because the

vertical wheel loading are not the same (see the measured loads shown on the very last

page of this report) bearing in mind the low speed at which the vehicle was travelling.
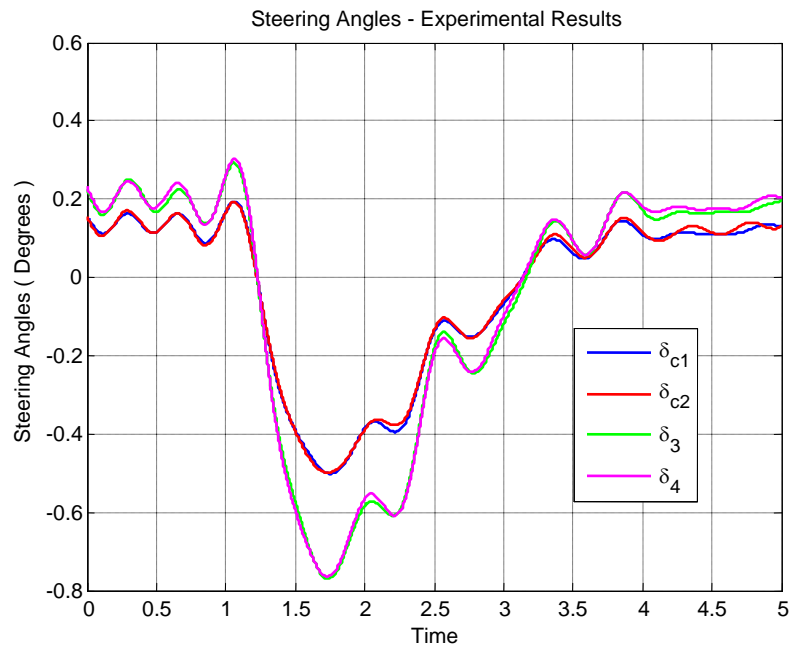

Figure 6-11:   Steering angles responses to braking at 40 km/h

Figure 6-11 shows the steering angles recorded while disturbing the vehicle with braking

from 40 km/h. It shows that all the wheels managed to return to zero steer position

though quite slowly.

7   CONCLUSIONS AND FUTURE WORK

The research work has measured and presented some results, of which the conditions to make a full correlation study between measurement and numerical prediction is not known, but at least the work can show simulation results that quantitatively look quite similar, and the conditions that pertain to this simulation is quite realistic, i.e., it would have been possible to have made an experiment with matching conditions.

It can be noted from the theories presented that under dissimilar conditions at the wheels, in order to give a true picture of the actual vehicle, every wheel has to be treated individually. When one is driving or steering, wheels are in contact with the ground independently. Even the load (weight) distribution of the vehicle is not the same on all the wheels as evidenced from the measurement results of the experimental vehicle. When wheels are not treated as a single entity, like in the bicycle model, some information is bound to be lost. In this dissertation a steering control analysis has been presented, similar to that of Ackermann, but with each wheel treated on its own. In addition to this, the modelling of a side wind acting at the centre of pressure was included in the analysis. The model that has been investigated is clearly an improvement of the bicycle model that has been used extensively by researchers in the understanding the concepts of 4WS. The results from simulations indicate that now it is possible to control each wheel independently. We have seen an improvement in the vehicle response by individually controlling the wheels as compared to the conventional steering. With control laws based on the bicycle model, the vehicle tends to oscillate, especially at lower coefficients of friction. The independent steering control laws in this work were shown to result in larger stability margins (fewer oscillations) even at lower coefficients of friction. The cases that

were investigated in this work are generic in that they were not condition specific, because it is now possible to investigate different road conditions at the left and right hand side wheels.

From the results presented, the wheels are able to return to their zero steering angle position after the effect of a disturbance was rejected. It was important to make sure that no steering angle remains after action of the control system. This highlights the ability of this experimental vehicle to reject disturbances.

There were some problems with the experimental results obtained. The results were deficient in terms of repeatability because of the configurations and characteristics of the wiper motors used. Firstly, there were slight differences between clockwise and anti-clockwise characteristic responses of the wiper motors used. Secondly, at low speeds, the motors could not push hard enough to generate the required angles. Another problem was that the yaw rate sensor used had significant inherent noise. Otherwise, given all conditions to be ideal, with this method, there is a possibility to achieve disturbance rejection.

Since one of the objectives was to be able to steer the wheels individually, and this was met, one can take advantage of that to further the research. On the experimental side, it will now be easier to let the wheels be on different road conditions and monitor the performance. More also, one can do further tests like subjecting the vehicle to different road manoeuvres e.g. double lane changes, parallel parking, and side gust response measurements, if side wind generating tunnels were to be made available. Future work can benefit from employing more suitable actuators, because the type of motors that were

used were essentially underpowered and the performance and response of the motors in clockwise and anticlockwise directions were observed to be different. One can also think of improving the system modelling by using the equations in their nonlinear form, especially with respect to simulation, and see if there will be any improvements (or perhaps deteriorations) compared to the linearized equations analysis. The extension of this work into nonlinear regime should also look at more sophisticated tyre models. The vehicle dynamics modelling also needs to be expanded to include roll dynamics, with the associated load transfer. This will be important if manoeuvres like double lane changes were to be simulated. More also, the control laws [4.13] to [4.18] that were investigated in simulations, assumed that the friction coefficient at each wheel is known. It is, however, quite difficult (if not impossible) to measure, in real time, the friction coefficient in order to implement these control laws. This is one of the major disadvantages of the proposed control laws. Therefore, one can also do a research and look into practical ways on how to estimate the friction coefficient, if the uses of these control laws are to be further employed.

REFERENCES

Abe, M. (1999). V*ehicle dynamics and control for improving handling and active safety: from four wheel steering to direct yaw moment control*. Proc Instn Mech Engrs. Vol. 213 Park K, pp. 87-101.

Abe, M., and Mokhiamar, O. (2002). *Active wheel steering and yaw moment control combination to maximize stability as well as vehicle responsiveness during quick lane change for active vehicle handling safety.* Proc Instn Mech Engrs, Vol. 216 part D: J Automobile Engineering, pp. 115-124.

Ackermann, J. and Bunte, T. (1997). *Yaw disturbance attenuation by robust decoupling of car steering.* Control Engineering Practice, (pp.1131-1136).

Ackermann, J., (1992) *Robust yaw damping of cars with front and rear wheel steering*, Proceedings of the 31st Conference Declalon and Control, Tucson, Arizona, pp. 2586-2590.

Ackermann, J., Bunte, T., and Odenthal, D. (1999). *Advantages of active steering for vehicle dynamics control*. Proc. 32nd International Symposium on Automotive Technology and Automation, pages 263-270, Vienna.

Ackermann, J. and Bunte, T. (1995). *Automatic car steering control bridges of the driver reaction time.* Institute for robotics and system dynamics, Germany.

Ackermann, J. and Bunte, T. (1996). *Driving safety by robust steering control*. Proc. Int. Symposium on Advanced Vehicle Control, (Aachen, Germany).

Ackermann, J., in co-operation with Blue, P., Bunte, T., Guvenc, L. Kaesbauer, D., Kordt, M., Muhler, M. and Odenthal D. (2002). *Robust control: The variable space approach*. Second Edition, Springer-Verlag.

Ackermann, J., Walter, W., and Bunte, T. (2004). *Automatic car steering using robust unilateral decoupling.* International Conference on Advances in Vehicle Control and Safety, Genoa, Italy.

Dorf, R.C. and Bishop, R.H. (2001). *Modern Control Systems, International Edition*. Ninth Edition. Prentice – Hall, Inc.

Friedland, B. (1986). *Control system design – An introduction to state space methods.* McGraw-Hill Publishing Company.

Ghelardoni, M. (2004). *Feasibility study of yaw control by active 4 - wheel drive*. Thesis, Technische Universiteit Delft.

Genta, G. (1997). *Motor vehicle dynamics – Modelling and simulation.* World Scientific Publishing Co. Pty. Ltd.

Gillespie, T.D. (1992) *Fundamentals of vehicle dynamics.* Warrendale, P.A., Society of Automotive Engineers.

Hanke, O. Bertram, T. and Hiller, M. (2001). *Analysis and control of vehicle dynamics under crosswind conditions.* IEEE/ASME International Conference on Advanced Intelligence Mechatronics Proceedings, Italy, pp 331 – 336.

Hucho, W.H. (1987). *Aerodynamics of road vehicles.* Butterworth. Printed in Great Britain at University Press, Cambridge.

Kitajima, K., and Peng, H. (2000). H_∞ *control for integrated side-slip, roll and yaw controls for ground vehicles.* Proceedings of Avec 2000 5th International Symposium on Advanced Vehicle Control, August 22-24, Ann Arbor, Michigan.

Klein, S. (1996). *Active control of a four wheel steered vehicle*. MEng. Dissertation, University of Pretoria.

Lakkad, S. (2004). *Modelling and simulation of steering system for autonomous vehicles.* Thesis, Florida State University, Collage of Engineering.

Lv H.M, Chenl, N. and LI P.I. (2004). *Multi-objective H_∞ optimal control for four wheel steering vehicle based on yaw rate tracking*. Proc. Institution of Mechanical Engineers, Vol. 218 Part D, Automobile Engineering, pp. 1117-1123.

Lynch, D.P. (2000). *Velocity scheduled driver assisted control of a four wheel steer vehicle.* Thesis, University of Illinois at Urbana-Campaign.

National Semiconductor Corporation, (2005). LMD18200 3A, 55V H-Bridge.

SAE J670e (1976). *Vehicle dynamics terminology.*

Wong, J.Y. (1993). *Theory of ground vehicles*. Second Edition, John Willy & Sons Inc.

Wu, D., Zhang, Q. and Reid, J.F. (2001). *Adaptive steering controller using Kalman estimator for wheel-type agricultural tractors.* Robotica Vol. 19, pp. 527-533. Cambridge University Press.

You, S.S., and Joeng, S.K. (1998). *Vehicle dynamics and control synthesis for four wheel steering passenger cars.* Proc Institution of Mechanical Engineers, Vol. 212 Part D, pp. 449-461.

Zhengqi, L., Yufeng, L. and Seemann, W. (2003). *The performance of a vehicle with four wheel steering control in cross wind.* International Journal Of Vehicle Autonomous Systems (IJVAS), Vol. 1, No. 2. pp. 256-269.

APPENDIX

Table B-1 shows experimental vehicle information. Some of the values here were from direct measurement of the vehicle while some of the values were calculated using available information that was gathered by Klein (1996).

Table B-1:   **Vehicle data**

Variable	**Description**	**Value**	**Unit**
$C_{\alpha 1}$	Front left cornering stiffness	12682	*N / rad*
$C_{\alpha 2}$	Front right cornering stiffness	11414	*N / rad*
$C_{\alpha 3}$	Rear left cornering stiffness	19023	*N / rad*
$C_{\alpha 4}$	Rear right cornering stiffness	20502	*N / rad*
m	Total mass	737	*kg*
l_f	Front axle distance to C.P.	0.678	*m*
l_{gp}	distance from C.G to C.P.	0.772	*m*
a	Front axle distance to C.G.	1.3	*m*
l_r	Rear axle distance to C.G.	1	*m*
l	Wheel base	2.3	*m*
t	Half track width	0.72	*m*
I_z	Yaw inertial	1320	*kgm^2*
h_{cg}	C.G. height	0.57	*m*

The values below are the static vertical wheel forces of the experimental vehicle that were found after measuring with wheel scales:

$F_{z1} = 146.03kgf$

$F_{z2} = 139.68kgf$

$F_{z3} = 210.431kgf$

$F_{z4} = 244.44kgf$